University of Potsdam
Faculty of Science
Geoecology

Master Thesis

Release and fate of organic and inorganic matter from the Batagaika thaw slump to the Yana River in central Yakutia (Russia) due to rapid permafrost degradation

Author:
Alessio Daniel Leins

Matrikel Nr. 784359

A thesis submitted in fulfillment of the requirements for the degree of Master of Science

supervised by

First Auditor	Dr. Michael Fritz
Second Auditor	apl. Prof. Dr. Bernhard Diekmann

April 2, 2019

Table of Contents

Statement of Authorship / Eigenständigkeitserklärung

I declare that I have authored this thesis independently based on my own work unless stated otherwise. All references and sources of information including graphs, data sets and pictures have been quoted or specifically acknowledged. No other person's work has been used without due acknowledgment in this thesis. Furthermore, I declare that this thesis has not been submitted for any other exam.

Berlin,

Ich versichere, diese Arbeit selbstständig und lediglich unter Benutzung der angegebenen Quellen und Hilfsmittel verfasst zu haben. Alle Stellen die wörtlich oder singemäß aus veröffentlichten oder noch nicht veröffentlichten Quellen entnommen sind, sind als solche kenntlich gemacht. Abbildungen in dieser Arbeit sind von mir selber erstellt worden oder mit einem entsprechenden Quellennachweis versehen. Außerdem erkläre ich, dass die vorliegende Arbeit nicht im Rahmen eines anderen Prüfungsverfahrens eingereicht wurde.

Berlin, den

List of Figures

List of Tables

Abbreviations

NH	Northern Hemisphere
Pg	Petagram; 1 Pg = 1 billion tons
a.s.l	Above sea level
MAGT	Mean annual ground temperature
YIC	Yedoma Ice Complex
MIS	Marine Isotope Stage
OSL	Optically-stimulated luminescence
IRSL	Infrared stimulated luminescence
ICP-OES	Inductively coupled plasma optical emission spectrometry
AMS	Accelerator Mass Spectrometry
MICADAS	Mini Carbon Dating System
PCA	Principal Component Analysis
PC	Principal components
EC	Electrical conductivity
CA	Cellulose acetate
DOM	Dissolved organic matter
DIM	Dissolved inorganic matter
DOC	Dissolved organic carbon
DN	Dissolved nitrogen
DON	Dissolved organic nitrogen
TOC	Total organic carbon
TIC	Total inorganic carbon

TC	Total carbon
TN	Total nitrogen
V-SMOW	Vienna Standard Mean Ocean Water
VPDB	Vienna Peedee Belemnite
GMWL	Global Meteoric Water Line
sd	standard deviation
min	minimum
max	maximum
C	Carbon
S	Sulphur
Al	Aluminum
Ba	Barium
Fe	Iron
Mn	Manganese
P	Phosphorus
Si	Silicate
Sr	Strontium
Ni	Nickel
Cu	Copper
Co	Cobalt
Zn	Zinc
CO_2	Carbon dioxide
CH_4	Methane
$NaHCO_3$	Sodium hydrogen carbonate
HCl	Hydrochloric acid
H_2CO_3	Carbonic acid
HNO_3	Nitric acid

$\mathbf{H^+}$	hydrogen ion / proton
$\mathbf{NH_4^+}$	Ammonium
$\mathbf{Na^+}$	Narium cation
$\mathbf{K^+}$	Sodium cation
$\mathbf{Mg^{2+}}$	Magnesium cation
$\mathbf{Ca^{2+}}$	Calcium cation
$\mathbf{NO_2^-}$	Nitrite
$\mathbf{NO_3^-}$	Nitrate
$\mathbf{HCO_3^-}$	Hydrogen carbonate anion
$\mathbf{CO_3^-}$	Carbonate anion
$\mathbf{Cl^-}$	Chloride anion
$\mathbf{SO_4^{2-}}$	Sulphate anion

Abstract

With ongoing climate change, permafrost soils and their function as carbon sinks are becoming more important as they might become carbon sources with rising global air temperatures. Landscapes are also changing, forming distinct features such as retrogressive thaw slumps, which not only release large amounts of organic carbon but also nitrogen, heavy metals, trace elements, major ions, sediment and fresh water into the environment depending on the regional settings. This thesis examines the release of dissolved and particulate matter due to the permafrost thaw in the Batagaika mega thaw slump in central Yakutia (Russia) (67°34'41.83" N, 134°45'46.91" E) and how it affects the subsequent streams the Batagaika and Yana River. In total 11 samples were taken: 5 slump, 4 Batagaika River and 2 Yana River samples, representing the flow path from the slump to the Yana River. The samples were analyzed for electrical conductivity, hydrogen carbonate content, DOC, nitrogen, major ion concentrations, heavy and trace metals, stable oxygen, hydrogen and carbon isotopes and were dated using radiocarbon measurements. When available, particulate matter in suspension was analyzed for total carbon, total organic carbon, total nitrogen and stable carbon isotopes, and were radiocarbon dated. The results show a significant release of dissolved organic and inorganic matter in the thaw slump affecting the water chemistry of the Batagaika River but showing no observable impact on the Yana River. Particulate matter does not seem to have had a strong impact on the subsequent rivers as sediment contents in suspension in the slump are >50 % and <2 % in the Batagaika and Yana River. Also TOC values are clearly lower in the slump compared to the Batagaika River. Trying to relate radiocarbon ages, stable isotopes and TOC values with specific stratigraphical units and ice wedges of the slumps headwall showed a connection to the upper sand unit of the NNE headwall and might lead to the conclusion of stronger erosion of a few units or sections of the headwall. However, the low sample resolution in this thesis both spatially and temporally must be considered in the interpretation of the results.

German Summary / Deutsche Kurzfassung

Im Zuge des globalen Klimawandels gewinnen Permafrostböden (Böden die für mindestens zwei aufeinanderfolgende Jahre gefroren sind) an Bedeutung. In Folge eines wärmeren Klimas tauen diese Böden auf und verlieren ihre Funktion als eine der größten terrestrischen Kohlenstoffsenken und werden zu Kohlenstoffquellen. Durch die mikrobiologische Umwandlung von organischem Kohlenstoff zu den Treibhausgasen Kohlenstoffdioxid und Methan, die in die Atmosphäre gelangen, wird der positive Rückkoplungszyklus durch auftauende Permafrostböden weiter angetrieben. Zudem werden durch das Auftauen weitere Stoffe wie Schwermetalle, Spurenelemente und Nährstoffe mobilisiert und gelangen in die Umwelt. Landschaftliche Auswirkungen machen sich unter anderem durch die Destabilisierung des Grundes bemerkbar, wodurch es zu Ablösung des oberen Bodens kommt und Erdrutsche verursacht werden. Dabei können sich Taurutschungen (retrogressive thaw slumps) bilden. In dieser Arbeit wurde die Freisetzung gelöster und partikulärer Stoffe durch die Permafrostrutschung im ,,Batagaika thaw slump“ in Yakutien (Russland) (67°34’41.83”N, 134°45’46.91”E) untersucht und wie sich dies im Abflussverlauf auf die nachfolgenden Flüsse, dem Batagaika und der Yana auswirkt. Insgesamt wurden 11 Proben mit enthaltenem Oberflächenwasser und suspendiertem Material bearbeitet. Fünf Batagaika Slump Proben, vier im Batagaika Fluss, einem Nebenfluss des Yana Flusses und zwei Proben im Yana Fluss. Die Orte der Probennahme geben den ungefähren Verlauf des Abflusses vom Slump bis zur Yana wieder. Im Labor wurden zuerst verschiedene hydrochemische Parameter wie elektrische Leitfähigkeit, Hydrogenkarbonatgehalt, gelöste organische und anorganische Stoffe sowie stabile Sauerstoff-, Wasserstoff- und Kohlenstoffisotope untersucht. Nach den hydrochemischen Untersuchungen wurden die Proben gefriergetrocknet, um das partikuläre Material auf den gesamten Kohlenstoffgehalt und dem organischen Kohlenstoffgehalt, gesamten Stickstoffgehalt und auf stabile Kohlenstoffisotope zu

messen. Radiokarbondatierungen wurden sowohl für gelösten als auch für partikulären Kohlenstoff durchgeführt. Die Ergebnisse weisen eine bedeutende Freisetzung von gelösten organischen und anorganischen Stoffen auf, die sich auf die hydrochemische Zusammensetzung des Batagaika Flusses auswirkt, jedoch keinen sichtbaren Einfluss auf den Yana Fluss nimmt. Die hohe Freisetzung von Sediment und infolge dessen einer hohen Sedimentfracht im Slump mit über 50 % wirkt sich nicht auf den Batagaika und Yana Fluss mit einer Sedimentfracht von weniger als 2 % aus. Die Konzentration von partikulärem Kohlenstoff und Stickstoff im Batagaika und Yana Fluss sind zudem höher als im Slump selber. Eine weitere Fragestellung der Arbeit war es, dass erodierte Material im Slump mittels der Datierung und anderer Parameter einer stratigraphischen Schicht des Slump-Aufschlusses (slump headwall) zuzuweisen. Dieser kann Mächtigkeiten bis zu 80 m erreichen und weist mehrere stratigraphische Einheiten auf. Die Untersuchung ergab einen stärkeren Zusammenhang zu einer der oberen Schichten (upper sand). Dennoch ist es wichtig, die Ergebnisse mit Vorsicht zu betrachten. Die geringe Anzahl der Proben und der Umstand, dass es sich um eine einmalige Probennahme handelt, schließt die Betrachtung zeitlich bedingter Dynamiken aus.

1 Introduction

1.1 Thematic Background

1.1.1 Permafrost

Permafrost is defined as frozen ground which remains at or below 0 °C for at least two consecutive years (Van Everdingen, 2005) beneath the land surface (terrestrial permafrost) as well as beneath the sea floor (subsea permafrost). In this thesis the term permafrost refers to terrestrial permafrost. It occurs at high latitudes in non-glaciated Arctic and Antarctic regions as well as in mountain regions (Fig. 1) (IPCC, 2013; Vaughan et al., 2013; Brown et al., 1997). The Northern Hemisphere (NH) permafrost underlies approximately 22.79 x 106 km^2 or 23.9 % of the exposed land area, extending from 26°N in the Himalayas to 86°N in northern Greenland (Zhang et al., 2008). Permafrost temperatures in the NH range from -15 °C to close to the freezing point, depending on the latitude and proximity to warm ocean currents (Romanovsky et al., 2010b). Permafrost can be distinguished by its continuity as shown in Fig. 1. This includes continuous permafrost, where more than 90 % of the area is permafrost, discontinuous permafrost (50-90 %), sporadic permafrost (10-50 %) and isolated patches (<10 %) (Brown et al., 2002). It can also be classified by its ice content. An ice content higher than 25 vol% permafrost ground is called ice-rich permafrost, while less than 25 vol% ice-poor (Brown et al., 2002). Permafrost ground usually consists of three subsurface units. On top lies the active layer, characterized by seasonal thaw during summer and refreezing in winter (Schuur et al., 2008). Thus even in permafrost regions plant growth and decomposition takes place (Van Everdingen, 2005). Active layer thickness in the continuous permafrost zone ranges from a few millimeters to more than 2 m, whereas in the discontinuous zone, it can reach several meters (Schuur et al., 2008). Underneath the active layer lies the transition zone, which consists of an ice-rich layer, separating the active layer from the more stable permafrost below (Shur et al., 2005). Permafrost depths can reach up to 1450 m below surface in Eastern Siberia (Schuur

et al., 2008). Permafrost has also the role as carbon (C) sink in context of climate change (IPCC, 2013). Approximately 1672 petagrams (Pg; 1 Pg = 1 billion tons) C are stored in the northern circumpolar permafrost zone (Schuur et al., 2008) of which 800 Pg are stored in permafrost (Hugelius et al., 2014). The C density in permafrost is typically higher near the surface because organic C originates from photosynthesis and plant growth (Schuur et al., 2008). However, due to cryogenic (freeze-thaw) mixing and sedimentation, organic C pools can also occur in larger scales at higher depths (Schirrmeister et al., 2002; Zimov et al., 2006)).

Permafrost temperatures have increased in most regions over the last number of years (high confidence) (IPCC, 2013; Vaughan et al., 2013). Differentiating between cold permafrost (ground temperature below -2 °C) and warm permafrost (ground temperature above -2 °C) (Cheng and Wu, 2007; Smith and Riseborough, 2010; Wu et al., 2010), permafrost temperature increase is higher in cold permafrost than in warm permafrost (high confidence) (IPCC, 2013; Vaughan et al., 2013). Permafrost warming responds mainly to an increase of air temperature and change of snow cover (IPCC, 2013; Vaughan et al., 2013). By the end of the 21st century climate models project an increase of mean annual air temperature in the Arctic by up to 8.3 ± 1.9 °C (Collins et al., 2013). Permafrost warming will result in two main consequences: First, in the degradation of permafrost which refers to a decrease in thickness and/or areal extent (IPCC, 2013; Vaughan et al., 2013), leading to increased thermokarst related mass movement, changes in hydrological pathways and threatening infrastructure due to the destabilization of the soil (Lantuit and Pollard, 2005; Boike et al., 2012; Jorgenson et al., 2006; Nelson et al., 2001). Second, an impact on ecosystems on a local scale and on climate on a global scale, due to the release and mobilization of previously stored organic carbon in frozen soil, referred to as permafrost carbon feedback (Schaefer et al., 2014; Hugelius et al., 2014; Schuur et al., 2008). Due to the warming induced environmental changes the microbiological breakdown of organic carbon into the greenhouse gases carbon dioxide (CO_2) and methane (CH_4) accelerates, which are released into the atmosphere (Schuur et al., 2015).

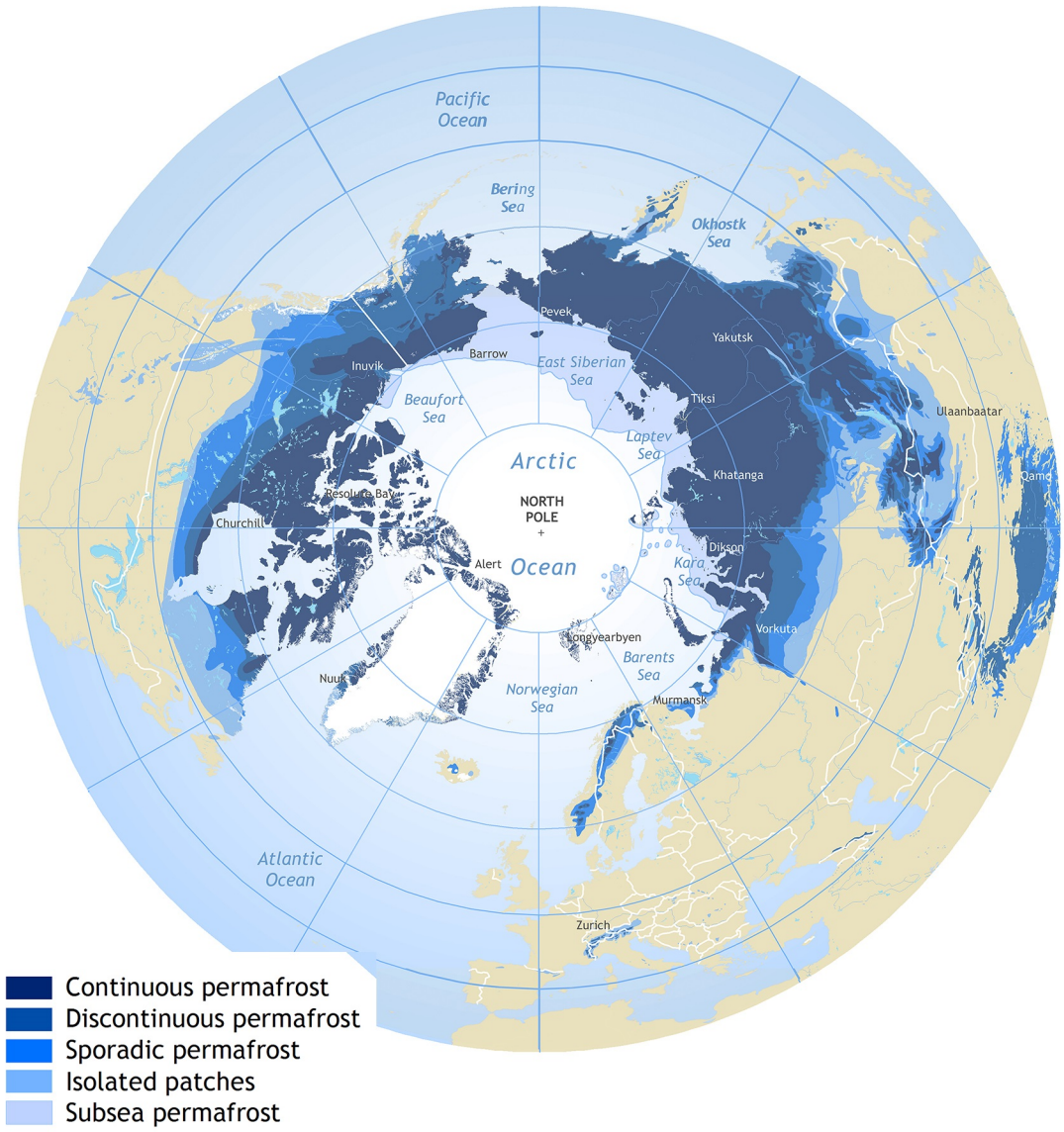

Figure 1 Circumpolar map of the different permafrost zone distribution of the northern hemisphere (Brown et al., 1997).

1.1.2 Thermokarst and Retrogressive Thaw Slumps

Thermokarst is the process of thawing ice-rich permafrost, causing land subsidence, resulting in the formation of distinctive landforms (Olefeldt et al., 2016). These landforms can be distinguished in three major categories: (1) wetland thermokarst landscapes including thermokarst bogs, fens and shore fens; (2) lake thermokarst landscapes characterized by lake initiation, expansion, drainage and drainage basin development; (3) and hillslope thermokarst landscapes, which include active layer detachment slides, retrogressive thaw slumps, thermal erosion gullies, beaded streams and thermokarst water tracks (Olefeldt et al., 2016). Retrogressive thaw slumps are characteristic features in ice-rich permafrost regions. They are thermal erosional C-shaped depressions (Fig. 2) caused by the thawing of exposed ice-rich permafrost on steep slopes and the removal of sediment by wave or fluvial erosion along the coast, lakes and rivers (Lantuit et al., 2012). Ablation of the headwall is caused by climate factors such as air temperature, solar radiation, wind speed, rain, debris and snow cover (Lewkowicz, 1986). Warmer air temperatures and direct exposure to solar radiation leads to high ablation, whereas layers of snow and debris protect the ice (Lewkowicz, 1987). Currently the frequency of retrogressive thaw slumps occurrence is increasing (Lantuit and Pollard, 2005), leading to the release of large amounts of organic carbon, nitrogen, sediment and freshwater into the environment (Lantuit and Pollard, 2005; Keuper et al., 2012; Kokelj et al., 2013). Due to this release of organic matter and nutrients, changes on the biogeochemistry and food-webs in aquatic systems could be a major consequence (Abbott et al., 2015; Kokelj et al., 2013; Malone et al., 2013; Moquin et al., 2014). In comparison to other thermokarst features, carbon losses in retrogressive thaw slumps are higher. In addition the long-term change of the landscape affects the vegetation, which can take decades or centuries to recolonize, leaving bare ground more susceptible to erosion (Cray and Pollard, 2015).

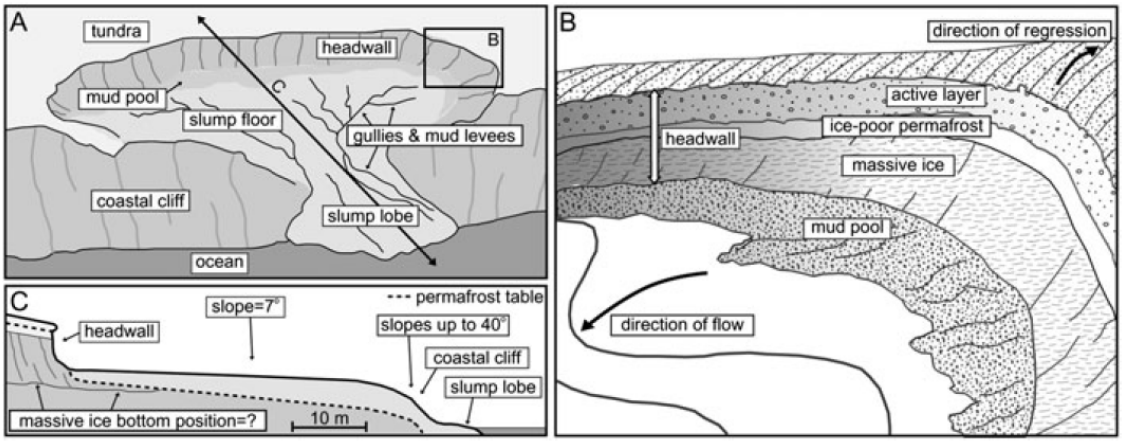

Figure 2 **(A)** Conceptual drawing of a retrogressive thaw slump; **(B)** generalized stratigraphy of the slump headwall; and **(C)** cross-section of the slump. Taken from Lantuit and Pollard (2005)

1.1.3 Aims and Objectives

The aim of this thesis is to asses the release of organic and inorganic matter from the Batagaika thaw slump in central Yakutia (Russia), whose discharges from the slump into the Batagaika River further into the Yana River. Furthermore, several isotope analyses such as radiocarbon dating, stable water and carbon isotopes should give an overview of where the material from the headwall is eroding from. The specific objectives of the thesis are:

1. Quantifying the organic and inorganic matter released from the thaw slump and how it behaves along the flow path to the Yana River in both dissolved and particulate matter form.
2. Dating and tracing back the source of erosion from the slump headwall with radiocarbon and stable isotope data.
3. Comparing the data with results of other fieldwork conducted on the Batagaika slump.

2 Study Site

2.1 Location

As described in Ashastina et al. (2017b) the Batagay mega thaw slump (67°34'41.83" N, 134°45'46.91" E) (Fig. 3) is located in the Siberian Yana Highlands about 10 km southeast of the village of Batagai, which is the municipal centre of the Verkhoyansk district, Sakha Republic (Yakutia) (Fig. 4). It lies on the left bank of the Batagay river, and descends to an altitude between 300 and 240 m above sea level (a.s.l.) into the foothills of Mt. Khatyngnakh, which are 381 m high. The Batagai slump drains into the Batagay River which is a tributary to the Yana River (Murton et al., 2017). The coast of the Laptev Sea lies 420 km north of the study site.

2.2 Geology

The region is part of the western Verkhoyansk-Kolyma orogen, which is characterized by the occurrence of Tertiary dark grey terrigenous siltstone and argillite, and mudstone that has undergone low-grade metamorphism (Vdovina, 2002), containing layers of sands forming crumpled and broken sediment packs with intrusive rocks (Ashastina et al., 2017b). The Neogene is represented by clay deposits interspersed with pebbles and gravel, loam, sandy loam and sands (Ashastina et al., 2017b), while Quaternary deposits are present as discontinuous layers covering older beds of hard rock and dispersed rocks (Kunitsky et al., 2013). The mean annual ground temperature (MAGT) is -7.7 °C (Romanovsky et al., 2010a) with a permafrost depth ranging from 200 to 500 m (Yershov, 2004).

Figure 3 Overview of the Batagay mega-slump, Batagay region Russia 67°34'41.83" N, 134°45'46.91" E, 27 May 2016, viewed 28 June 2018. Taken from Google Earth Pro version 7.3. Image ©2018 CNES / Airbus.

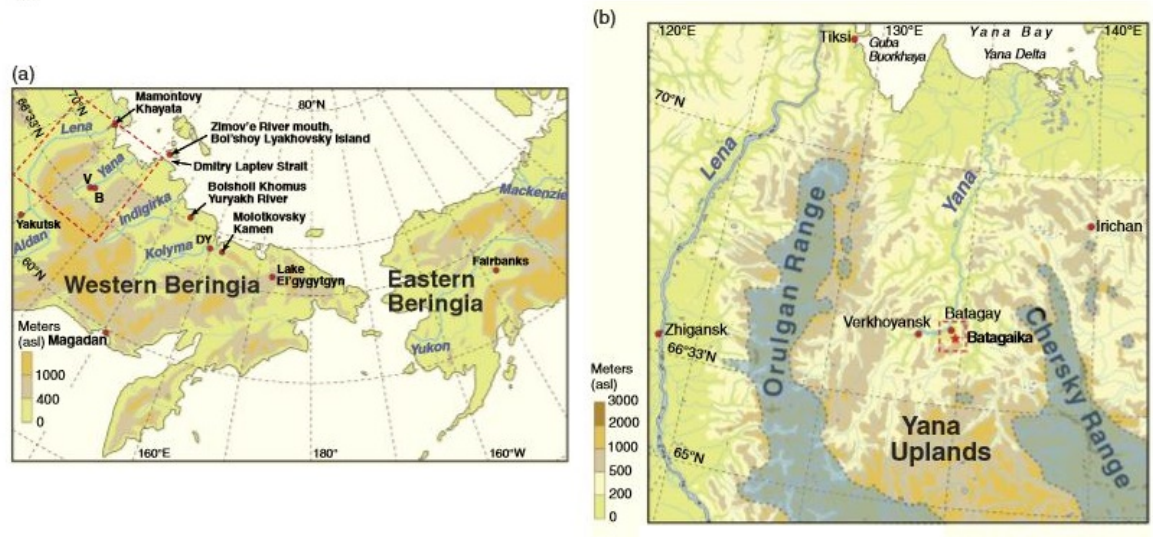

Figure 4 Location maps of the Yana River in western Beringia **(a)** and Batagaika within the Yana River basin **(b)**. Taken from Murton et al. (2017).

2.3 Climate

According to the classification of Köppen (1884) the climate is continental subarctic, which is characterized by low precipitation, great seasonal temperature gradient (in lower latitudes diurnal) forming under the influence of a large landmass and a great distance to the sea. According to data from Verkhoyansk weather station, which has been recording since 1888, it is the region with the greatest recorded temperature range on earth. The mean July air temperature is +9.9 °C while in January it is -38.7 °C (Fig. 5). The absolute recorded winter minimum is -67.8 °C and the absolute summer maximum is +37.3 °C, which results in a temperature range of 105.1 °C. The absolute winter minimum of -67.8 °C is accepted as the lowest temperature measured in the northern Hemisphere (Lydolph, 1985; Ivanova, 2006). The mean annual precipitation is 231 mm, with the lowest rates during winter and the highest during summer (https://de.climate-data.org/location/761428/. Accessed November 5, 2018).

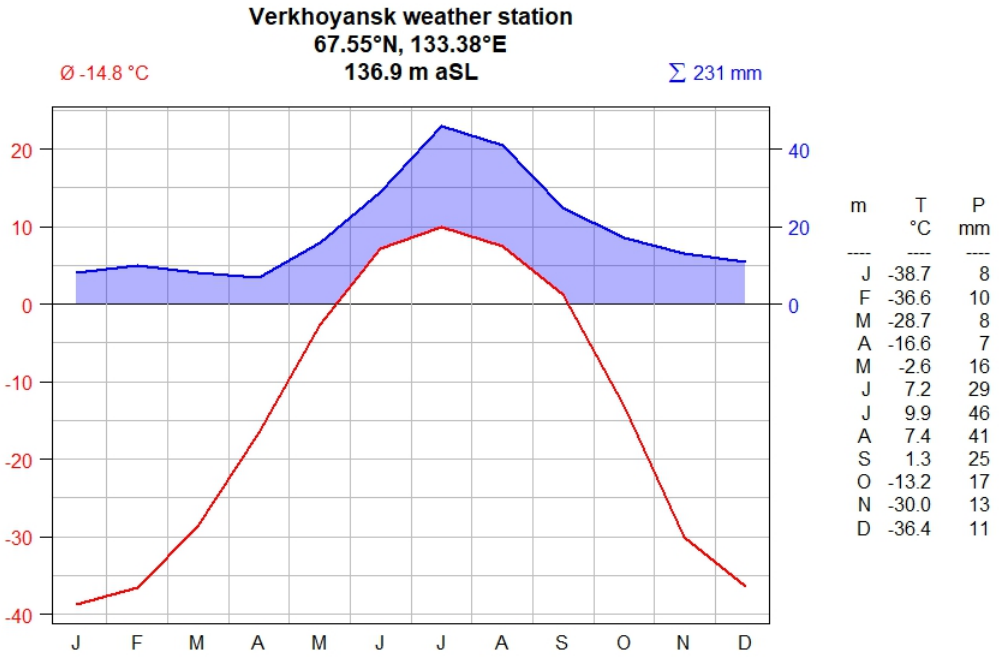

Figure 5 Climate graph after Walther and Lieth showing the mean monthly temperature in red and mean monthly precipitation in blue. The blue shaded area symbolizing humid periods (Precipitation > Evaporation). The graphic was generated in R with the "berryFunction" package (Boessenkool, 2017).

2.4 Morphology and Lithostratigraphy

The Batagay thaw slump (Fig. 3) is a erosion sink 800 m in diameter, with up to 80 m steep faces, which formed during the last 40 years (Ashastina et al., 2017a). The part of the slump that is most actively eroding is the southwestern end, which consists of nearly vertical walls (Ashastina et al., 2017b) (Fig. 6a). The walls of the southeastern part have a gentler slope with a gradient up to 45°(Ashastina et al., 2017b) (Fig. 6b). It is the biggest thermo-erosional thaw slump worldwide (Günther et al., 2015). At least two times larger than any previous described thaw slump, it has been the subject of recent cryostratigraphical analysis (Kunitsky et al., 2013). As a palaeoclimate archive it exposes a profile of Yedoma deposits. Yedoma is described as organic-rich permafrost by Zimov et al. (2006) (2 % to 5 % C by mass), which suggests that a third to one half of all OC in permafrost is stored in Yedoma deposits. At the Batagaika thaw slump Yedoma deposits reach a thickness of 7 to 22 m (Slagoda, 1991) underlaid by ice-rich periglacial alluvial sand deposits of around 60 m thickness (Kunitsky et al., 2013). Vertical drainage channels have been formed by meltwater and mud flow off the steep slopes along the western and southern parts (Ashastina et al., 2017b). The height difference between the headwall and outflow of the slump into the Batagay River is 145 m along a distance of 2300 m with a current size of >81 ha, while it thawed $>24.2 \times 10^6$ m^3 of ice-rich permafrost in 2014 (Günther et al., 2015). Due to this inclination the meltwaters streams into the Batagaika River forming a fan with ridges up to 30 m high of frozen sediments (Ashastina et al., 2017b). Thermo-denudation is occurring with rates up to 15 m per year (Günther et al., 2015).

The Batagay headwall consists of distinct stratigraphic units (Ashastina et al., 2017b; Murton et al., 2017). Unit I represents the active layer, also referred to as the Holocene layer, and does not show a constant thickness along the Batagay outcrop, with a maximum depth of 1.4 m (Ashastina et al., 2017b). Radiocarbon dating yielded an age of 0.259 ka BP (Ashastina et al., 2017b).

Unit II (upper sand) is up to about 20 m thick and represented by narrow syngenetic and composite ice wedges surrounded by pore-ice cemented brown to grey sand (Opel et al., 2018). AMS ages range between 36.30 ± 0.70 and 26.18 ± 0.22 ka BP (Ashastina et al., 2017b; Murton et al., 2017), corresponding to deposition during MIS 3 and MIS 2 (Opel et al., 2018). Unit III (upper Ice complex) corresponds

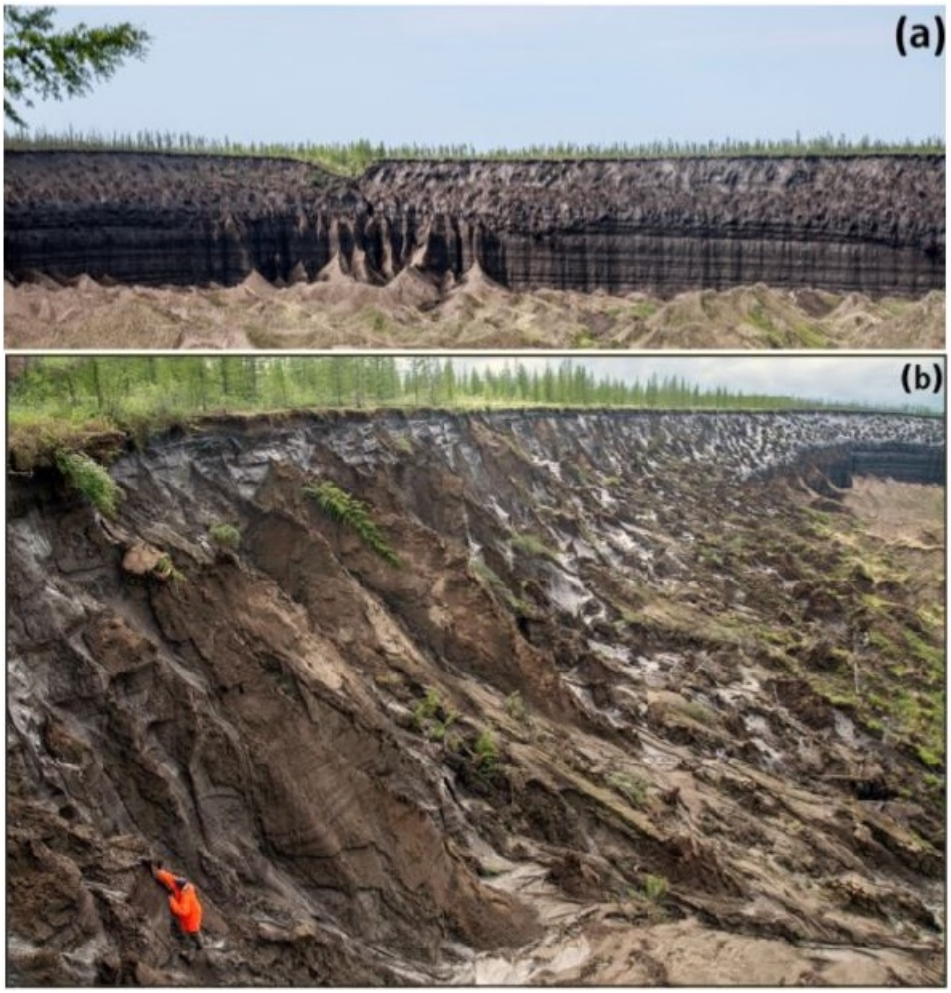

Figure 6 **(a)** Total view of the southwestern slump wall. **(b)** Southeastern slope of the slump. Note person for scale. Pictures taken from (Ashastina et al., 2017b).

to the Yedoma Ice Complex (YIC) and is about 20 to 40 m thick with 4.5 to 6.5 m wide ice wedges within silty and sandy deposits (Ashastina et al., 2017b; Opel et al., 2018). AMS radiocarbon ages from > 51 to 12 ka BP (Ashastina et al., 2017b) indicate deposition during MIS 3 to late MIS 2 (Opel et al., 2018). The range of > 51 to 12 ka BP with large gaps in Unit III suggests that the sedimentation experienced interruption or partial erosion of sequences (Ashastina et al., 2017b). The upper ice complex (Unit III) forms the highest stratigraphical unit in the upper central part of the slump headwall, while towards the slump mouth further downwards it is partially overlain by the upper sand (Unit II) (Murton et al., 2017; Opel et al., 2018; Ashastina et al., 2017b).

Unit IV (organic rich layer) is 1.5 m thick and characterized by a high abundance of macroscopic plant material, including woody remains (Ashastina et al., 2017b). Proxy records together with radiocarbon ages of this unit (> 44 ka BP) indicate a formation of Unit IV during the MIS 5e interglacial (Ashastina et al., 2017b).

Unit V (lower sand) is 20 to 30 m thick with tall, narrow syngenetic ice wedges (up to 0.5 m) within yellowish pore-ice cemented fine sand with grey horizontal bands (Opel et al., 2018). Optically-stimulated luminescence (OSL) dated the middle part of the unit to 142.8 ± 25.3 and >123.2 ka, infrared stimulated luminescence (IRSL) to 210.0 ± 23.0 ka (Ashastina et al., 2017b), corresponding to a deposition during MIS 6 (Marine Isotope Stage) or even MIS 7.

Unit VI (lower Ice complex) at the bottom of the slump wall is 3 to 7 m thick and contains syngenetic ice-wedges within pebbly dark sand (Opel et al., 2018). The ice wedges let assume the formation of this layer occurred in a cold-stage climate during the middle Pleistocene (781 ka BP to 126 ka BP), surviving at least two glacial-interglacial cycles (MIS 5 and MIS 1) Ashastina et al. (2017b).

3 Methods

3.1 Sample Locations

A total of eleven samples were collected during field work in late July to early August 2017 (Tab. 1). An overview of the sampling locations are shown in Fig. 7. Samples 01, 02, 03, 06 and 08 were taken from inside the slump. Samples 08 and 02 represent the slump main drainage channel ending with 06 at the slump outflow to the Batagaika River (Fig. 8a). Samples 01 and 03 are side streams which at some point converge with the slump main drainage channel. Sample 04 was taken 5-6 km downstream of the slump outflow in the Batagaika river. Samples 07 and 05 are from the Batagaika River directly up- (07) and downstream (05) of the mouth from the slump outflow into the river (Fig. 8a). Sample 10 represents the outflow of the Batagaika River into the Yana River, while 09, 11 are Yana River samples 50 m down- (09) and upstream (11) of the Batagaika outflow. For 08, 09, 10 and 11 no exact coordinates were collected. The locations were determined by interpreting the description of the sample location and checking the satellite image (Fig. 8b). Samples 09, 10 and 11 were collected by a local environmental agency.

Figure 7 Overview of all sample locations represented as red dots. Taken from Google Earth Pro version 7.3. Image Landsat / Copernicus. Image ©CNES / Airbus. Viewed 8 March 2019.

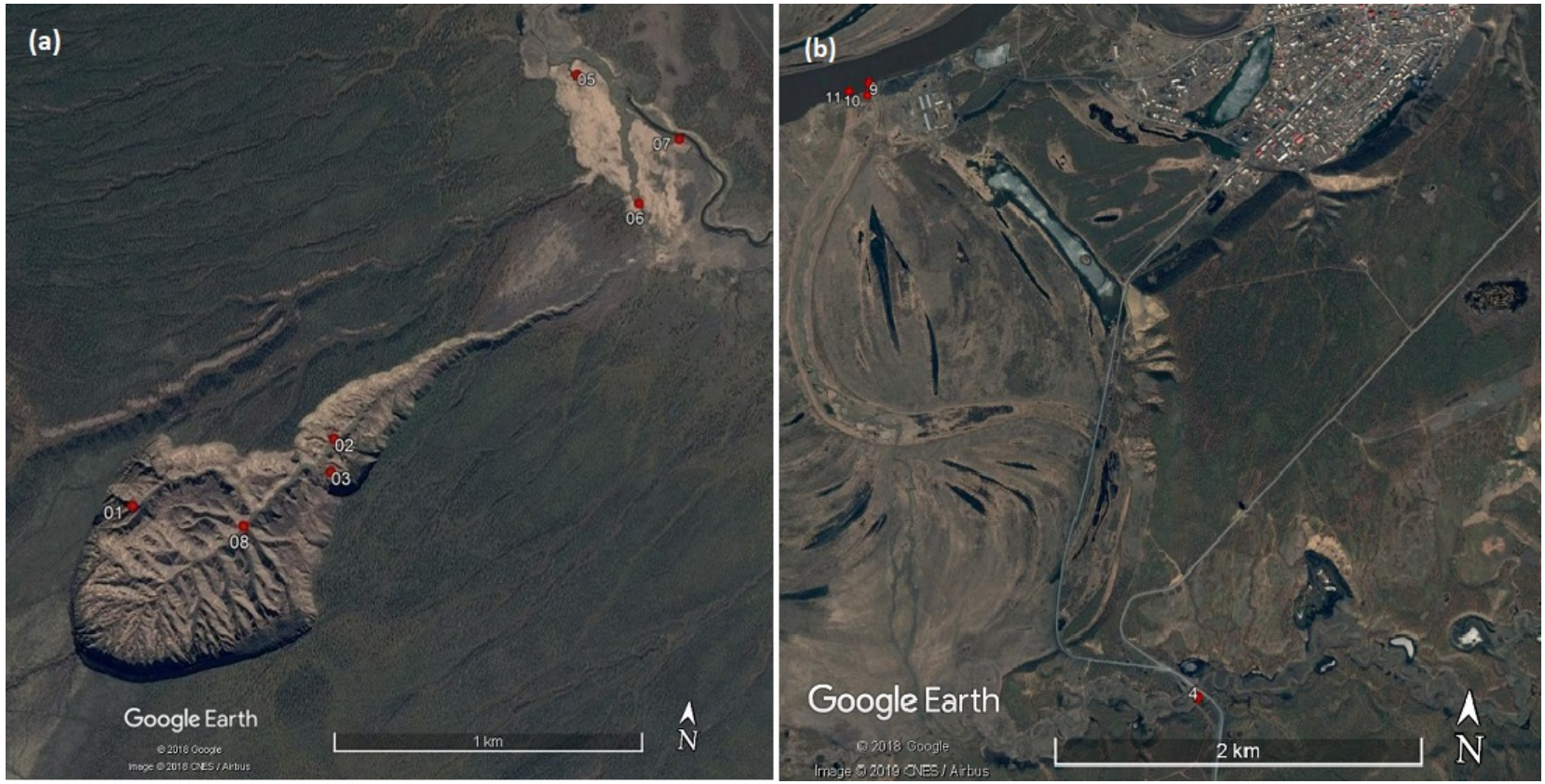

Figure 8 **(a)** Overview of samples 01, 02, 03 and 08 taken from the slump and 06 (slump outflow), 07 (Batagaika upstream), 05 and 04 (Batagaika downstream), **(b)** 10 (Batagaika outflow), 11 (Yana upstream) and 09 (Yana downstream) represented as red dots. Taken from Google Earth Pro version 7.3. Image ©2018 CNES / Airbus. Viewed 9 August 2018 and 8 March 2019.

Table 1 Sample positions and dates of sampling campaign

Sample ID	Date	LAT (°N)	LONG (°E)	Sample Position
B17-MF-01	28.07.2017	67 34' 53.1"	134 45' 57.6"	small stream draining a part of the headwall
B17-MF-02	29.07.2017	67 35' 02.7"	134 46' 54.1"	main outflow of stream (downstream of all major creeks)
B17-MF-03	29.07.2017	67 34' 59.0"	134 46' 52.2"	stream draining the secondary headwall in the south of the slump
B17-MF-04	31.07.2017	67 37' 10.9"	134 36' 41.1"	Batagaika river 5-6km downstream of slump outflow
B17-MF-05	31.07.2017	67 35' 49.4"	134 47' 56.5"	Batagaika River downstream of slump outflow
B17-MF-06	31.07.2017	67 35' 34.0"	134 48' 17.6"	Slump outflow
B17-MF-07	31.07.2017	67 35' 42.4"	134 48' 29.0"	Batagaika River upstream of slump outflow
B17-MF-08	31.07.2017	-	-	Stream draining the SW part of the slump, ca 30 m upstream of unification with other stream to build the main stream
B17-MF-09	-	-	-	Yana River, 50 m downstream of Batagaika River
B17-MF-10	-	-	-	Batagaika River
B17-MF-11	-	-	-	Yana River, 50 m upstream of Batagaika River

3.2 Hydrochemistry

The measurement of pH and electrical conductivity (EC) provides the first insights of the samples in terms of acidity and the content of total dissolved solids. Usually the EC increases with higher ion concentration in the water. The pH and EC were measured with a MultiLab 540 Labor-WTW. For the analysis 7 ml were pipetted from unfiltered samples.

Major anion and cation analysis provides a quantification of major inorganic ions in water such as chloride (Cl^-), sulphate (SO_4^{2-}), sodium (Na^+), potassium (K^+), magnesium (Mg^{2+}) and calcium (Ca^{2+}), as well as heavy metals. Therefore 30 ml from each sample were extracted with a syringe and filtered through a disposable 0.45 µm pore size millipore cellulose acetate (CA) filter unit (Whatman® AQUA 30/0.45 CA filter unit white rim). Overall 22 (2 x 11) subsamples were extracted. For cation analysis 8 ml sample into 15 ml centrifuge tubes and 8 ml into 10 ml H/LDPE wide mouth bottles for the anion analysis. To prevent microbiological activity 50 µl of 65 % supra-pure nitric acid (HNO_3) were added to each cation subsample. The anion samples were frozen. Cations and heavy metals were measured through inductively coupled plasma optical emission spectrometry (ICP-OES) with a Perkin Elmer Optima 8300 DV. Anion concentrations were measured through ion-chromatography (IC) using an DIONEX/Thermo ICS-2100. Anion and cation were measured at the Alfred-Wegener-Institute in Potsdam. The results of the anion and cation analyses are presented in a Piper-Plot (Piper, 1944). For the visualization in a Piper-Plot Eq. 1 was used on the data. The mass concentrations in $mg \cdot l^{-1}$ of major cations (Na^+, K^+, Ca^{2+}, Mg^{2+}) and anions (Cl^-, SO_4^{2-}, HCO_3^-) had to be transformed in equivalent concentration in $mmol \cdot l^{-1}$ for the distinction with the molar concentration (expressed as $mmol(eq) \cdot l^{-1}$). Cations and anions are illustrated in ternary diagrams as the percentage fraction of the respective ions. In addition, both ternary diagrams are projected into a rhomb to distinguish different water types. Error ranges due to measurement precision are ± 10 %.

$$c_{(\mathrm{eq})} = c \cdot \frac{z}{M} \tag{1}$$

$c_{(\mathrm{eq})}$	equivalent concentration	mmol(eq) l^{-1}
c	mass concentration	mg l^{-1}
z	valence of the ion	
M	molar mass	mg $mmol^{-1}$

For dissolved organic carbon (DOC), total dissolved nitrogen (DN), δ^{13}C-DOC, nitrate (NO_3^-), nitrite (NO_2^-) and ammonium (NH_4^+) analyses, 200 ml from each sample were extracted with a syringe and filtered through a disposable GF/F 0.7 µm pore size glass microfiber filter unit (Whatman® Glass Microfiber GF/F). The filters were previously flushed with 30 ml ultra-pure water to flush out any potential remains of dissolved organic matter. Sixty milliliters of the samples were sent to the University of Hamburg for DN, NH_4^+, NO_3^- and NO_2^- analyses. Forty milliliters were leveled into 60 ml and 40 ml Vial Clear Boro w/Septa 72/cs and acidified with 60 µl and 40 µl 30 % supra-pure hydrochloric acid (HCl) to prevent microbiological activity. The remaining 100 ml were leveled into brown glass bottles. For each of the three sample series a blank with ultra-pure water was made to detect background concentrations. Dissolved organic nitrogen (DON) was calculated by subtracting NH_4^+, NO_3^- and NO_2^- from the total amount of dissolved nitrogen. The DOC analyses were conducted at the Alfred-Wegener-Institute in Potsdam with a TOC-VCPH Shimadzu.

The titration to calculate the dissolved hydrogen carbonate (HCO_3^-) concentration was made with the 794 Basic Titrino Metrohm. A volume of 2 ml extracted from the 8 ml sample for anion analysis was titrated with a 0.01 M HCl solution. Due to the hydrochemical carbonate balance, where HCO_3^- in solution reacts to carbonic acid (H_2CO_3) (Fig. 9) with decreasing pH until 4.3 because no more HCO_3^- is solved, the titration stopped automatically at that pre-setted mark. Based on the HCl consumption the HCO_3^- concentration in mg l^{-1} could retrospectively be calculated (Eq. 2). Previous to the titration of samples two standards, 500 µmol l^{-1} and 2000 µmol l^{-1} of 1 mol l^{-1} sodium hydrogen carbonate ($NaHCO_3$), were titrated. The error range of this method is ± 10 % (Wisotzky, 2011).

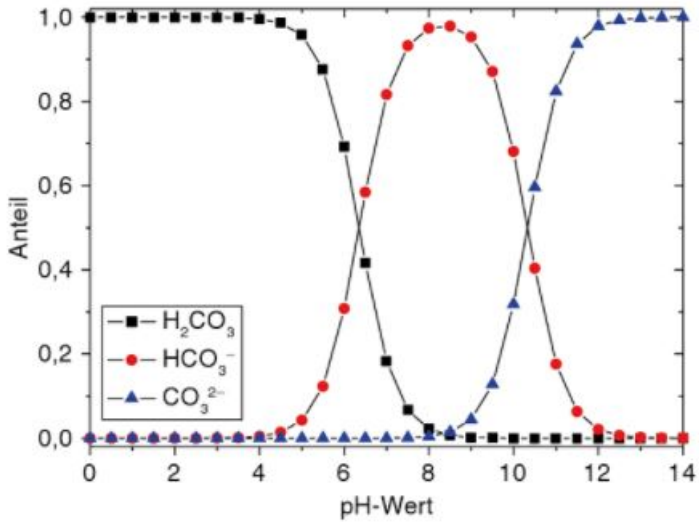

Figure 9 Portion of carbonic acid (H_2CO_3), hydrogen carbonate (HCO_3^-) and carbonate-ion (CO_3^-) (y-axis) of water sample in dependency of the pH (x-axis) from Wisotzky (2011).

$$c = \frac{V_{\mathrm{HCl}} \cdot M_{\mathrm{HCl}}}{1000} \tag{2}$$

c	hydrogen carbonate concentration	mg l^{-1}
V_{HCl}	consumed hydrochloric acid	µmol l^{-1}
M_{HCl}	molar mass of hydrochloric acid	61.015 g mol^{-1}

3.3 Stable Water Isotopes

Stable water isotopes can give insights into the climate of the past. Cold and warm stages as well as the distance from sources of evaporation and precipitation have different impacts on the isotope composition. With higher global temperatures the amount of heavier atmospheric oxygen and hydrogen isotopes increases due to more energetic evaporation, which then is transported to the polar regions.

Ten milliliters of unfiltered sample were pipetted into 30/10 ml PE narrow neck bottles for $^{18}O/^{16}O$-water and $^{2}H/^{1}H$-water isotope analysis at the Alfred-Wegener-Institute in Potsdam with a Finnigan-MAT Delta S mass spectrometer. Through the ionization of the compound into gas-phase ions, the molecular ions are sepa-

rated according to their mass-to-charge ratio and then detected in proportion to their abundance, resulting in a production of a mass spectrum. (De Hoffmann and Stroobant, 2007).

The isotope abundance is expressed through the relative difference of the isotope ratio of a compound to that of an international standard (Werner, 2003). The international standard for oxygen and hydrogen isotope ratio measurements is the Vienna Standard Mean Ocean Water (V-SMOW), according to international agreement (Gonfiantini et al., 1995). The oxygen and hydrogen isotopes ratio was calculated as shown in Eq. 3 and Eq. 4. In addition, the deuterium excess (d excess), which is an indicator for non-equilibrium fractionation processes, was calculated after Dansgaard (1964) Eq. 5. These fractionation processes are generally related to humidity, sea surface temperature and wind speed in the initial source region as well as evaporation in the target region (Meyer et al., 2010). The results can be plotted in a co-isotope δ^{18}O-δD diagram with respect to the Global Meteoric Water Line (GMWL; Eq. 6), which shows a linear correlation of global fresh surface waters (Craig, 1961). Minimum, mean and maximum values, standard deviation (sd) as well as slope and R^2 where calculated. The internal errors are 1σ ranging between 0.1 and 0.4 for δ^2H and 0.01 to 0.03 for δ^{18}O.

$$\delta^{18}O[‰]_{\text{V-SMOW}} = \left[\frac{(\,^{18}O/^{16}O)_{\text{sample}}}{(\,^{18}O/^{16}O)_{\text{V-SMOW}}} - 1\right] \cdot 1000 \tag{3}$$

$$\delta D[‰]_{\text{V-SMOW}} = \left[\frac{(\,^{2}H/^{1}H)_{\text{sample}}}{(\,^{2}H/^{1}H)_{\text{V-SMOW}}} - 1\right] \cdot 1000 \tag{4}$$

$$d = \delta D - 8 \cdot \delta^{18}O \tag{5}$$

$$\delta D = 8 \cdot \delta^{18}O + 10 \tag{6}$$

3.4 Sediment Content and Dry Bulk Density

The weight of each sample was measured and subtracted with the mean weight from 8 other identical but empty sampling bottles including the bottle cap. The Volume (including solid matter) was determined by filling and comparing an identical sampling bottle with the sampled ones. After all hydro-chemical analyses were conducted the samples were freeze-dried. This process involves the dehydration of the samples by freezing them and afterwards lowering the pressure to remove the water by sublimation (water turning from the solid ice phase to the gaseous phase). Afterwards the samples were weighed again to calculate the sediment content (Eq. 7) and dry bulk density (Eq. 8).

$$x = \frac{M_{\mathrm{d}}}{M_{\mathrm{w}}} \cdot 100 \tag{7}$$

x	sediment content	%
M_{d}	dry sample mass	g
M_{w}	wet sample mass	g

$$p = \frac{M_{\mathrm{d}}}{V_{\mathrm{d}}} \tag{8}$$

p	dry bulk density	g cm^{-3}
V_{d}	dry sample volume	cm^3

3.5 Particulate Matter Analysis

In order to compare the dissolved matter with the suspended particulate matter regarding organic carbon and nitrogen as well as radiocarbon dating and stable carbon isotope analysis the samples were freeze-dried as described in chapter 3.4. Total organic carbon (TOC) was measured with a Vario MaxC, total carbon (TC) and total nitrogen (TN) with a Vario El III at the Alfred-Wegener-Institute in Potsdam. The total inorganic carbon (TIC) was calculated by subtracting the TOC from TC. The C / N ratio was calculated to derive the degree of organic matter

decomposition. With lower C / N ratios the degree of decomposition is higher and vice versa (White, 2013; Gregorich and Carter, 2007). The ratio was calculated using Eq. 9. Not enough material after the freeze-drying process and milling of the suspended sediment of sample 07 was left for analyses on this specific sample point. The DOC / DN ratio was also calculated with Eq. 9 using the DOC and DN values. For samples 07 (Batagaika River upstream of the slump outflow), 09 (Yana River downstream of the Batagaika outflow) and 11 (Yana River upstream of the Batgaika outflow) the DN were below the detection limit of 0.5 mg/l; thus no DOC / DN ratios could be calculated.

$$C/N = \frac{TOC/M_{\mathrm{C}}}{TN/M_{\mathrm{N}}} \tag{9}$$

C/N	carbon-nitrogen ratio	
TOC	total organic carbon	%
M_{C}	molar mass of carbon	14 g mol^{-1}
TN	total nitrogen	%
M_{N}	molar mass of nitrogen	12 g mol^{-1}

3.5.1 Stable Carbon Isotopes

Stable δ^{13}C isotope data presents the ratio between the stable carbon isotopes ^{13}C and ^{12}C which gives information about previous native vegetation of the region (Bernoux et al., 1998). Using Eq. 10 data is presented in ‰ vs. VPDB (Vienna Peedee Belemnite). δ^{13}C ratios on TOC were measured with a ThermoFischer Delta V at the Alfred-Wegener-Institute in Potsdam. Therefore the samples were decalcified to remove any carbonate. Each subsample was heated to 97.7 °C for three hours in 20 ml of 1.3 mol/l HCl in 100 ml Erlenmeyer glass flasks and flushed with deionized water afterwards. Flushing and sedimentation was repeated three times in total to remove the Cl^- ions from the HCl and ensure pure isotope measurement. δ^{13}C-DOC ratios were measured at the University of Hamburg. Sample preparations were the same as for the determination of DOC concentrations described in Chapter 3.2.

In total 21 samples for δ^{13}C ratios were measured, of which 11 are DOC and 10 TOC due to the lack of particulate matter material in sample 07.

$$\delta^{13}C = \left[\frac{(^{13}C/^{12}C)_{\text{sample}}}{(^{13}C/^{12}C)_{\text{standard}}} - 1 \right] \cdot 1000 \tag{10}$$

3.5.2 Radiocarbon Dating

Accelerator mass spectrometry (AMS) ^{14}C radiocarbon dating provides an age estimate of the organic carbon in the sample. The ^{14}C-DOC dating was performed at the University of Cologne with an AMS mass spectrometer for seven samples: three slump samples (01, 08, 06), two Batagaika River samples (07, 05) and two Yana River samples (09, 11). They were filtrated into 250 ml HDPE wide mouth bottles, which where previously filled with 10 % HCl resting for 24 hours, than flushed to eliminate traces of organic matter. The filters with a pore size of 0.7 µm were pre-combusted at 550 °C. The filtration process was conducted with a Laboport® mini laboratory suction pump. 30 % supra pure HCl was than added to get the pH down to 2 - 3, controlled with pH paper, before freezing the samples to prevent microbiological activity. The ^{14}C-TOC dating was performed at the Alfred-Wegener-Institute in Bremerhaven by sending 200 mg of the suspended sample material, which was processed to pure graphite and then measured using Mini Carbon Dating System (MICADAS) mass spectrometer. The results are presented in uncalibrated and calibrated ^{14}C years. The calibration was calculated with the software Calib Rev 7.0.4 (Stuiver and Reimer, 1993) using IntCal13 (Reimer et al., 2013).

3.6 Data Analysis and Management

All data was analyzed and visualized with R Studio 1.1.383 (R Core Team, 2013). Additional packages used in R Studio are “ggplot2” (Wickham, 2016), “grid” (R Core Team, 2017), “gridExtra” (Auguie, 2017) and “berryFunctions” (Boessenkool, 2017).

3.7 Principle Component Analysis

Principal component analysis (PCA) reduces the dimensionality of the data set that consist of a large number of variables, while retaining most of the variation by transforming to principle components (PCs) (Jolliffe, 2011). PCs are uncorrelated and ordered as the variation they retain, usually the first few retain most of the variation in all of the original data set (Jolliffe, 2011). PCA in this thesis was done using R Studio packages "factomineR" (Lê et al., 2008) and "factoextra" (Kassambara and Mundt, 2017) to summarize the variation of parameters in the slump. The whole data set was reduced to 10 samples and 18 variables by removing those containing missing values.

4 Results

4.1 Hydrochemistry

4.1.1 Hydrogen Carbonate and Electrical Conductivity

For better graphical overview the samples are grouped according to the location they were taken from, as described in section 2.1. The highest values of HCO_3^- and EC are found in the slump. Values range between 812 mg/l and 1198 mg/l for HCO_3^- (Fig. 10a) and between 1651 µS/cm to 1937 µS/cm for electrical conductivity (Fig. 10b). After converging with the Batagaika River the concentrations decrease from 1198 mg/l for HCO_3^- and 1651 µS/cm for EC of the Slump outflow sample to 404 mg/l and 1285 µS/cm in the river. In comparison with the upstream samples of the Bagaika River (16 mg/l and 42 µS/cm) it shows a clear signal after the convergence of the two waters. Following the stream to the outflow into the Yana River the concentrations decrease to 228 mg/l and 395 µS/cm. The mixing of Batagaika and Yana River water does not show a detectable signal from the slump water, having HCO_3^- values from 36.2 mg/l before and 34.6 mg/l after mixing (Fig. 10a) and EC values of 120 µS/cm and 124 µS/cm (Fig. 10b).

4.1.2 Dissolved Organic Carbon

The highest DOC concentrations range from 158 mg/l to 173 mg/l (Fig. 11a), including six samples of which five are slump water and one Batagaika River water in immediate proximity downstream to the slump outflow with 164 mg/l. In contrast, the upstream value (4.87 mg/l) as well as both up- (4.25 mg/l) and downstream (4.38 mg/l) samples from the Yana River represent the lowest concentrations (Fig. 11a). The concentrations decrease further downstream in the Batagaika River after the initial mixing of slump and river water to 56.8 mg/l and 18.3 mg/l when the Batagaika flows out into the Yana River.

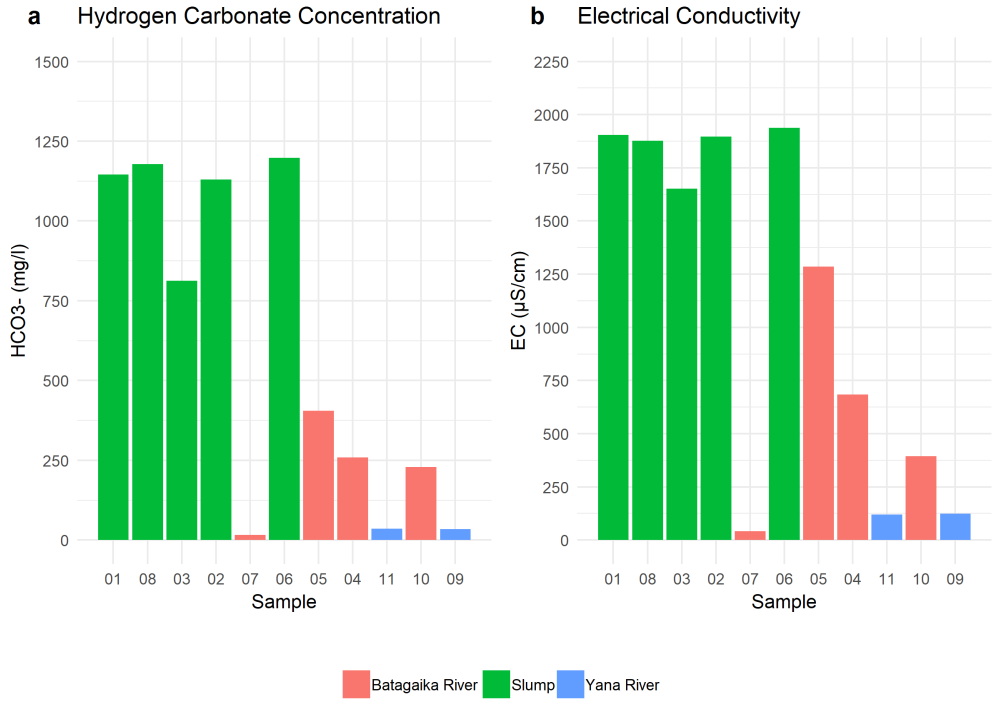

Figure 10 Bi-Carbonate concentrations **(a)** and electrical conductivity **(b)** color-coded by the locations slump, Batagaika and Yana River.

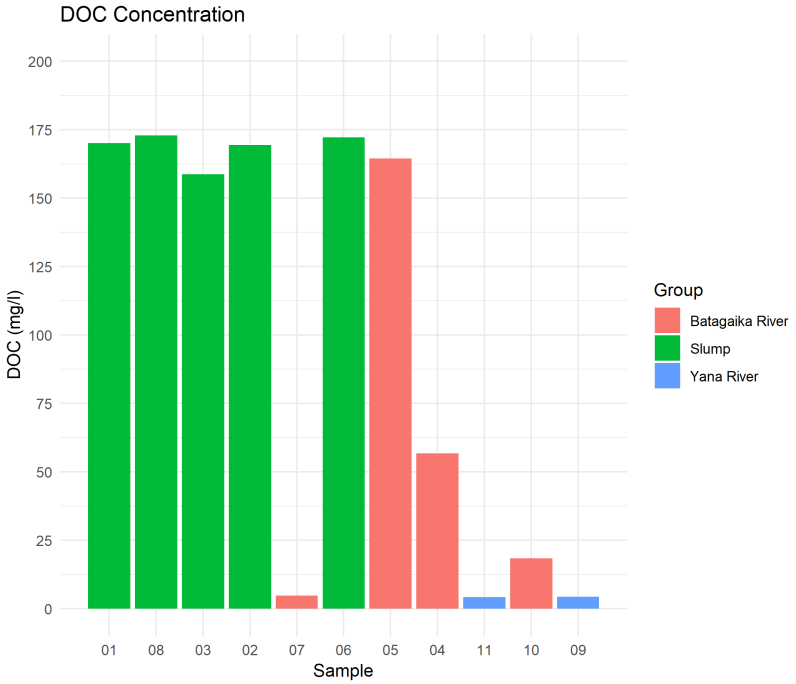

Figure 11 DOC concentrations color-coded by the location slump, Batagaika and Yana River.

4.1.3 Dissolved Nitrogen Components

Dissolved nitrogen was detected in all samples except for 07, 09 and 11 (Fig. 12a). Higher total nitrogen concentrations occur in the slump water, where the values range between 8.9 mg/l and 13.8 mg/l and sample 05 with 11.9 mg/l. Following the Batagaika River downstream the values decrease with 5.1 mg/l and 2.3 mg/l at the outflow of the Batagaika River (Fig. 12a). A similar succession can be seen in dissolved organic nitrogen (Fig. 12b). The highest values are found in the slump, ranging from 8.4 mg/l to 10.7 mg/l having a high DON signal after the mixing of the slump and Bataigaka water in 05, with 8.1 mg/l decreasing to 2.7 mg/l and 0.6 mg/l downstream the Batagaika River. High ammonia concentrations occur mostly in slump water or water directly affected by it (such as sample 05), with values from 3.3 mg/l to 3.8 mg/l (Fig. 13a). The rest of the samples show low concentrations ranging from 0.01 mg/l to 0.03 mg/l or too low for the method to be quantified (<0.01 mg/l), such as in sample 11 and 09 and slump sample 07 being the only slump grouped sample with such a distinct concentration in relation to the other slump waters. Nitrate concentrations are highest in the downstream and outflow part of the Batagaika River with 2.3 mg/l and 1.7 mg/l (Fig. 13b). Slump water values range from <0.014 mg/l to 0.5 mg/l. The Batagaika water before the mixing with the slump shows a concentration of 0.05 mg/l and <0.014 mg/l after mixing in sample 05. Yana River concentrations range from 0.06 mg/l to 0.12 mg/l. Nitrite concentrations resulted all in being below the device-specific detection limit.

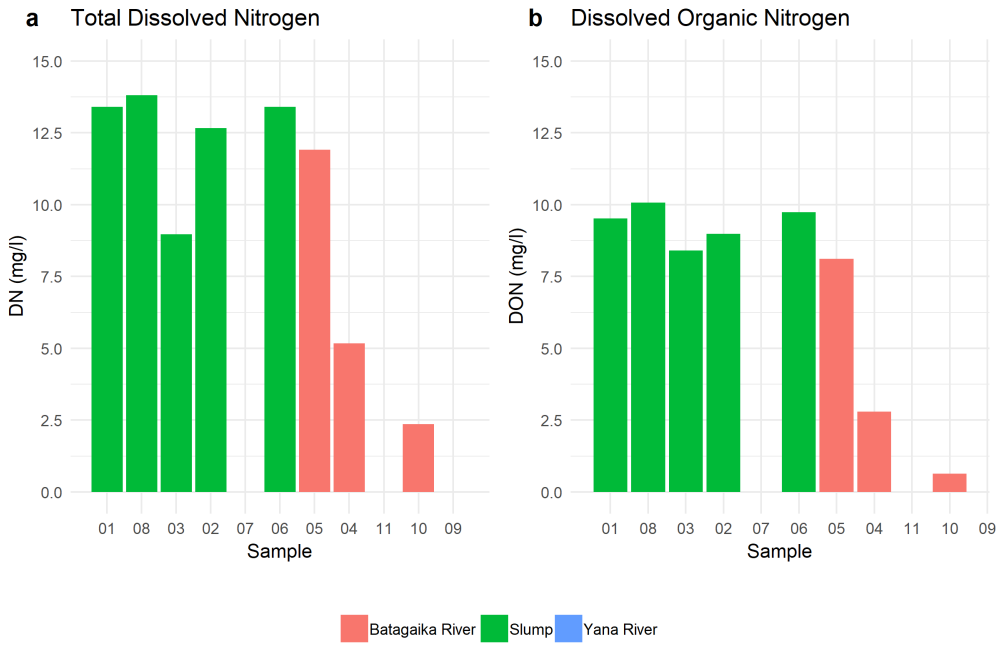

Figure 12 Total dissolved nitrogen **(a)** and dissolved organic nitrogen **(b)** concentrations color-coded by the locations Slump, Batagaika and Yana River.

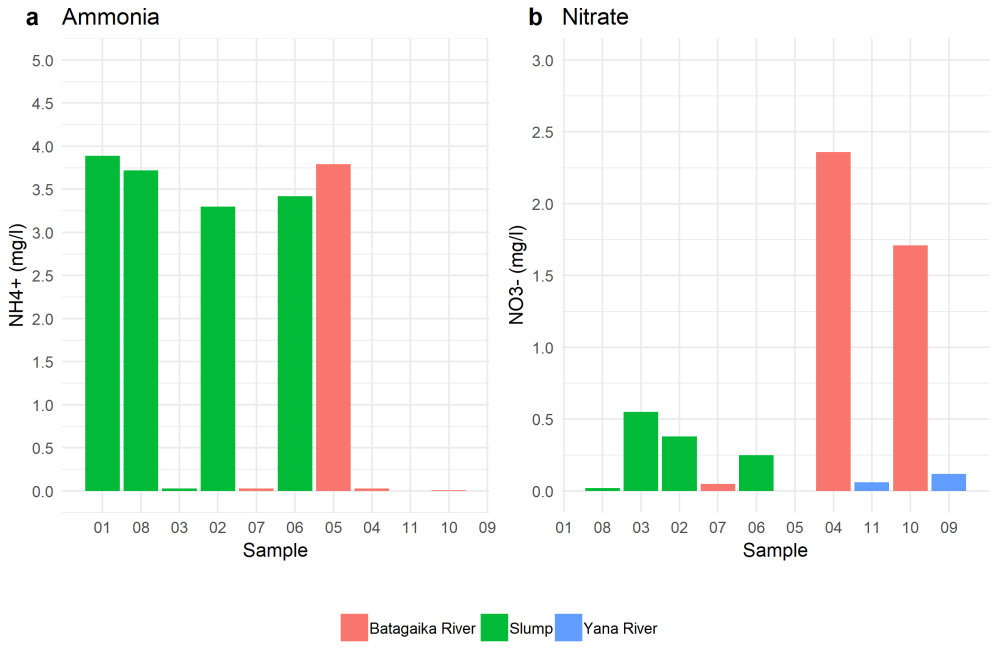

Figure 13 Ammonia **(a)** and nitrate **(b)** concentrations color-coded by the locations Slump, Batagaika and Yana River.

4.1.4 Major Anion and Cation Characteristics

All major anions and cations show a similar pattern regarding their concentrations from the slump to the Yana River. Slump waters have the highest values of Mg^{2+} (155 - 165 mg/l), Ca^{2+} (140 - 178 mg/l), Na^{+} (84 - 93.7 mg/l) and SO_4^{2-} (128 - 221 mg/l) (Fig. 14, Tab. 7). While K^{+} (5.04 - 5.41 mg/l) and Cl^{-} (64.4 - 67.3 mg/l) ion slump concentrations are also among the highest, directly after the slump outflow the concentrations are slightly higher with 6.63 mg/l K^{+} and 69.4 mg/l (Cl^{-}). In every case, ion concentrations of the Batagaika River are low before slump waters get mixed into it. Shown in Fig. 14 values increase significantly for Mg^{2+}: 1.78 mg/l to 83.5 mg/l, Ca^{2+}: 4.37 mg/l to 110 mg/l, Na^{+}: 1.63 mg/l to 81.9 mg/l, K^{+}: 0.44 mg/l to 6.63 mg/l, Cl^{-}: 1.15 mg/l to 69.4 mg/l and SO_4^{2-}: 4.62 mg/l to 264 mg/l. Flowing downstream they decrease for Mg^{2+}: 18.9 mg/l, Ca^{2+}: 60.9 mg/l, Na^{+}: 8.75 mg/l, K^{+}: 1.47 mg/l, Cl^{-}: 3.21 mg/l and SO_4^{2-}: 17.9 mg/l. The ion concentrations in the Yana River are below the concentrations of the Batagaika, except for SO_4^{2-} (Fig. 14, Tab. 7). However, in all cases the values slightly increase after the Batagaika waters flow into the Yana River. Final concentrations of the flow path are Mg^{2+}: 5.1 mg/l, Ca^{2+}: 15.3 mg/l, Na^{+}: 2.65 mg/l, K^{+}: 0.76 mg/l, Cl^{-}: 1.46 mg/l and SO_4^{2-}: 24.5 mg/l, showing an overall decrease of initial concentrations along the flow path.

The Piper diagram (Fig. 15) shows that the samples can be divided in three different water types. All slump samples as well as the Batagaika outflow into the Yana River and the Batagaika River upstream of the slump outflow are classified as earth-alkalic waters with a high hydrogen carbonate content and Yana River samples as earth-alkalic waters with hydrogencarbonatic-sulfatic content. The Batagaika River sample 6 km downstream from the slump outflow lies on the border of these two water types, while the Batagaika sample directly after the slump outflow can be classified as earth-alkalic water with high sulphate/chloride content.

Other traceable elements were Al, Ba, Fe, Mn, P, Si, Sr, Ni, Cu and Zn. However, Al, P and Cu were found only in few samples and mostly below the detection limit (Al and Cu: < 20 µg/l and P: < 0.1 mg/l) (Tab. 8), and thus are not plotted. Fe, Si and Sr show the same pattern along the flow path (Fig. 16), with the highest concentrations in slump waters (Fe: 1006 - 2279 µg/l, Si: 4.66 - 5.49 mg/l, Sr: 903 - 1110 µg/l). Batagaika River concentrations of Fe and Sr before the slump

outflow are 41 µg/l and 26.5 µg/l and increase significantly after the slump outflow to 762 µg/l and 630 µg/l. The Si concentrations from before and after the slump outflow also increase from 1.99 mg/l to 2.57 mg/l, however not as much in relation to Fe and Sr (Fig. 16). The Si does not decrease much downstream either (2.57 mg/l to 2.34 mg/l). Along the Batagaika River the values do not fluctuate or show a significant decrease. Furthermore, Yana River concentrations show a similar range before and after the Batagaika River water flows into the Yana River (Fig. 16c). Fe and Sr show a constant decrease from 762 µg/l and 630 µg/l in the Batagaika River after the slump outflow to 44 µg/l and 142 µg/l in the Yana River. Yana River water values before and after the Batagaika outflow do not change significantly (Fig. 16b and 16d). Zn concentrations in the slump range from 29 µg/l to 101 µg/l (Fig. 16e). The two lower values occur at the main drainage (08) and outflow (06) of the slump, while higher values (77 - 101 µg/l) occur near the slump walls. Upstream of the slump outflow the concentration is in the same range with 86 µg/l, decreasing to 31 µg/l directly after the slump outflow and further to 20 µg/l following the flow path. In the Batagaika outflow it increases slightly to 35 µg/l. Yana River samples were below detection limit of < 20 µg/l.

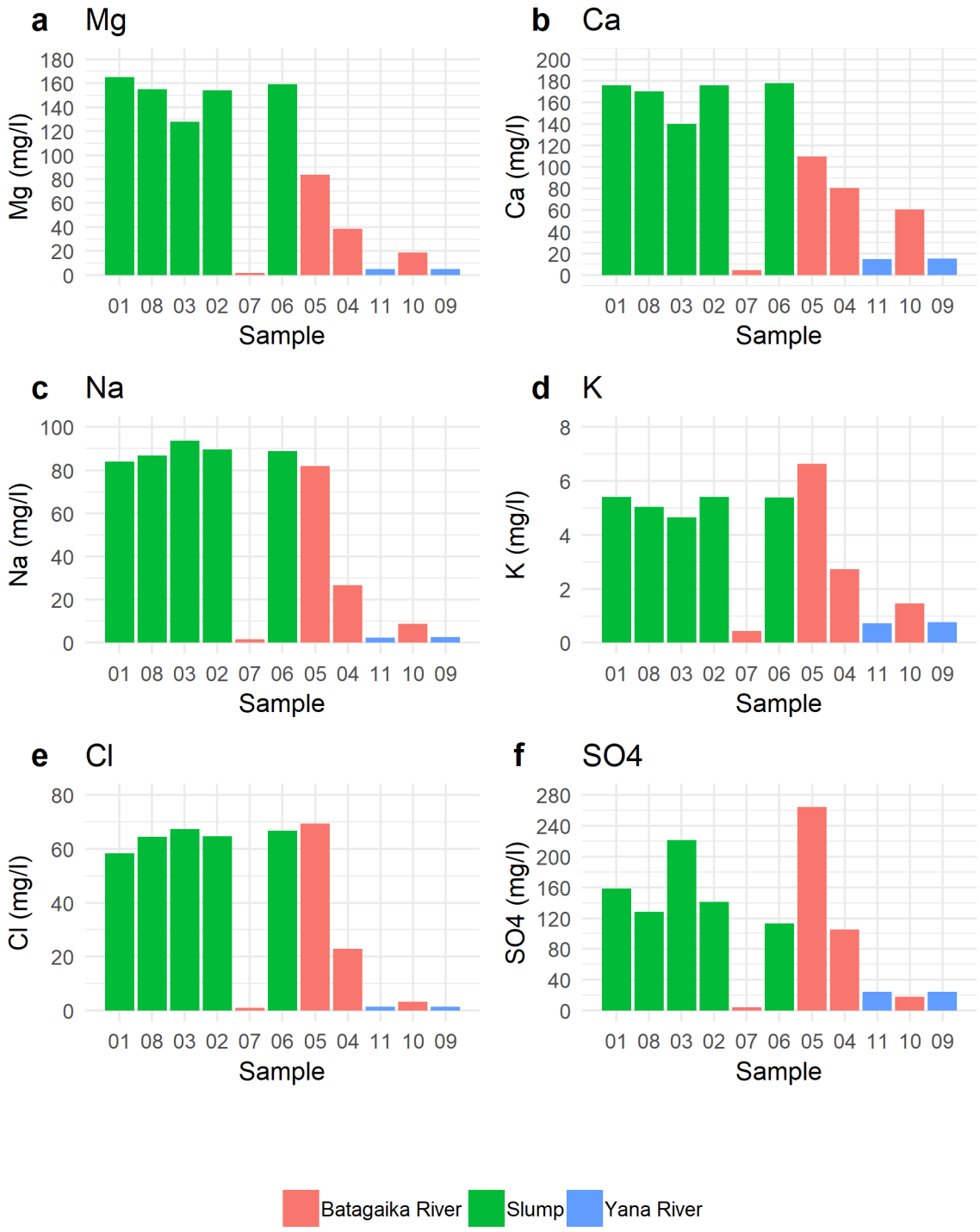

Figure 14 **(a)** Mg, **(b)** Ca, **(c)** Na, **(d)** K, **(e)** Cl and **(f)** SO_4 ion concentration in mg l^{-1} color-coded by the sample locations Slump, Batagaika and Yana River.

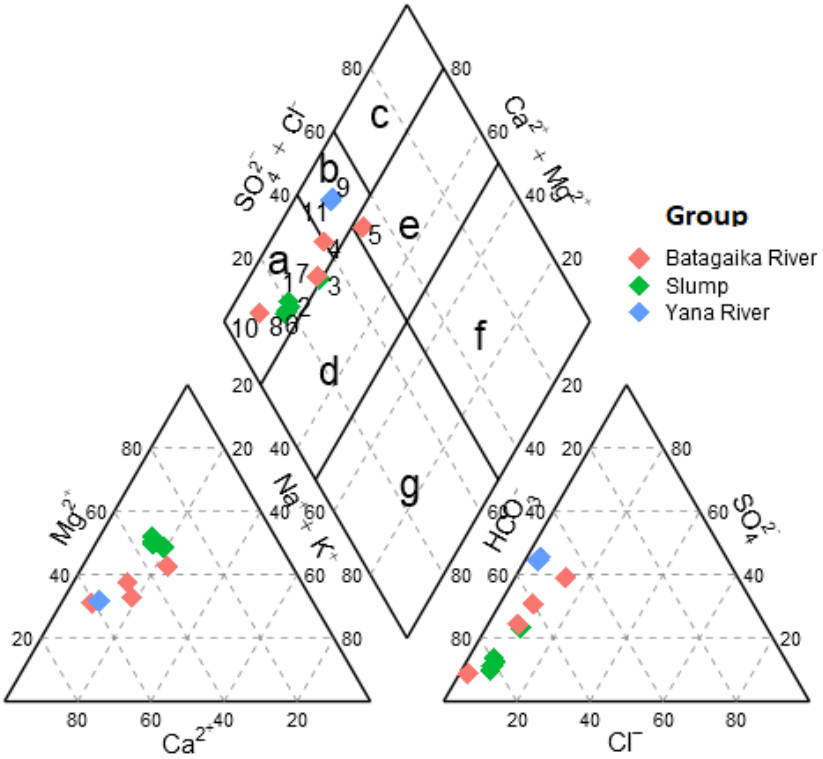

earth-alkalic

a	high hydrogen carbonate content
b	hydrogen carbonatic sulfatic
c	high sulfate content

earth-alkalic with higher content of alkali

d	high hydrogen carbonate content
e	high sulfate/chloride content

alkalic

f	high hydrogen carbonate content
g	high chloride content

Figure 15 Piper diagram with classification of different water types. Samples in the rhomb are numbered and color-coded after the sample location Slump, Batagaika and Yana River.

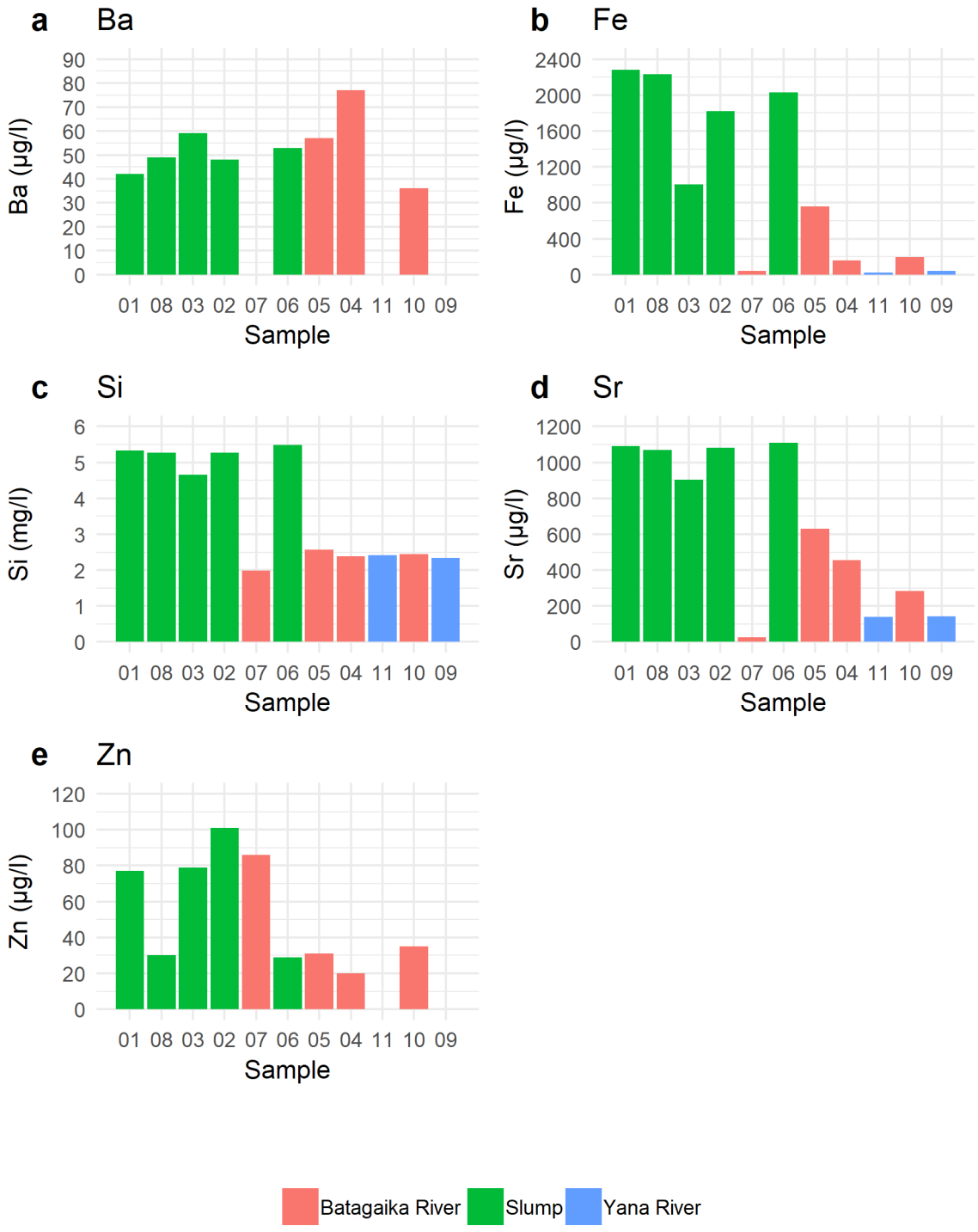

Figure 16 **(a)** Ba, **(b)** Fe, **(c)** Si, **(d)** Sr and **(e)** Zn concentrations color-coded by the sample locations Slump, Batagaika and Yana River.

4.2 Stable Water Isotopes

In Table 2, hydrogen and oxygen isotope minimum, mean, maximum values, standard deviations as well as slope, intercept and R^2 are given for all samples, Batagaika and Yana River samples and Slump stream water samples.

The isotopic composition throughout all samples ranges between -32.3 ‰ and -19.3 ‰ for $\delta^{18}O$ with a mean value of -26.7 ‰ and from -243.9 ‰ to -146 ‰ for $\delta^{2}H$ with a mean value of -202 ‰ (Fig. 17; Tab. 2). The d excess varies from 5.45 ‰ to 16.1 ‰ with a mean value of 11.5 ‰. Slope of 7.4 with an R^2 of 0.99 (Tab. 2). In the co-isotope diagram, two clusters separated from each other can be distinguished. Cluster 1 is represented by the slump water with lighter (most negative) ($\delta^{18}O$ mean of -31.5 ‰; $\delta^{2}H$ mean of -237 ‰; slope 5.9 and R^2 0.86). Cluster 2 is represented by Batagaika ($\delta^{18}O$ mean of -21.3 ‰; $\delta^{2}H$ mean of -164 ‰; slope 8.9 and R^2 0.99) and Yana River water ($\delta^{18}O$ mean of -21.3 ‰; $\delta^{2}H$ mean of -162 ‰; slope 10 and R^2 1) with heavier (most positive) isotopic composition (Fig. 17a). The signal of the lighter isotopes, all belonging to the slump samples (cluster 1), thins out as the slump water mixes with the Batagaika and Yana River (cluster 2) (Fig. 18a,b). Both clusters show a stable isotopic composition with variations of less then 3 ‰ for $\delta^{18}O$ and 21 ‰ for $\delta^{2}H$, respectively. Cluster 1 is situated slightly above, while cluster 2 is situated slightly below the GMWL (Fig. 17a), with mean d excess values of (14.67 ‰ for cluster 1; 6.82 ‰ for Batagaika water and 8.13 ‰ for Yana water), confirming the general assumption that the heavier the isotopic composition the lower d excess values. A succession of isotope composition from lighter slump water to heavier river water can be seen (Fig. 18a,b).

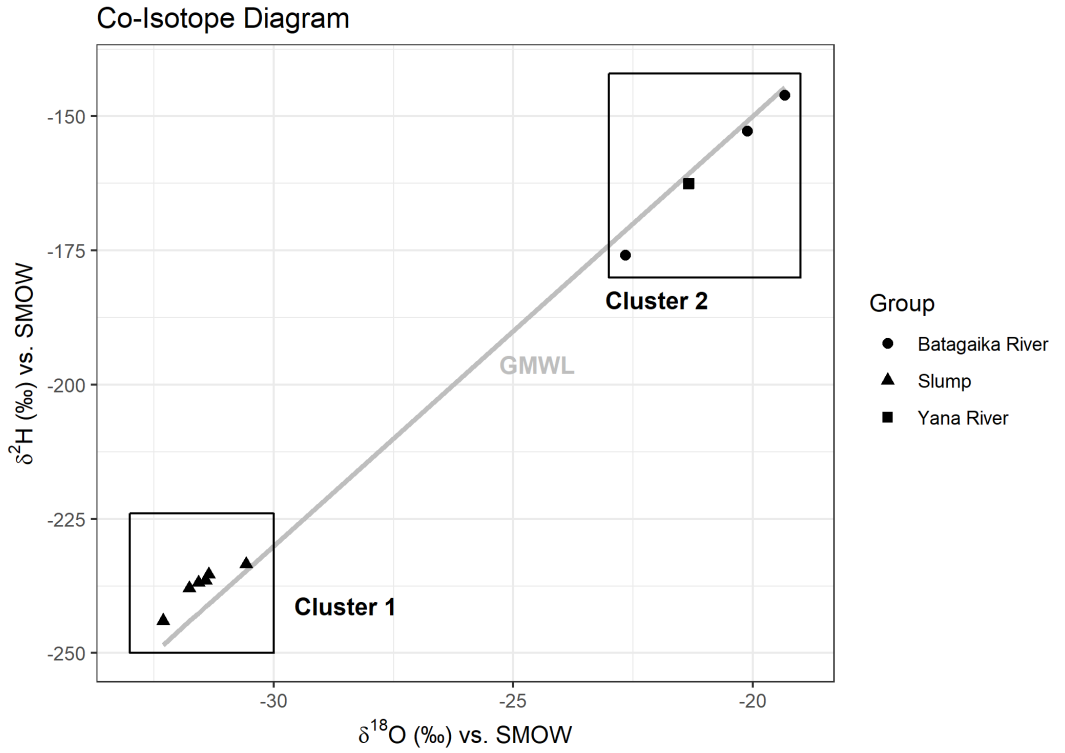

Figure 17 Co-isotope diagram where δ^2H is plotted against δ^{18}O and as grey line the Global Meteoric Water Line (GMWL). The black lined boxes mark cluster 1 (slump group) and cluster 2 (Batagaika and Yana River group).

Table 2 Summary of stable water isotopes (δ^{18}O, δ^2H and d excess), minimum, mean, maximum values, standard deviation (sd), slope, intercept and R^2 for the category all samples, Batagaika and Yana River water and slump water.

Group	N	δ^{18}O (‰) min	δ^{18}O (‰) mean	δ^{18}O (‰) max	δ^{18}O (‰) sd	δ^2H (‰) min	δ^2H (‰) mean	δ^2H (‰) max	δ^2H (‰) sd	d (‰) min	d (‰) mean	d (‰) max	d (‰) sd	slope	R^2
All Samples	11	-32.3	-26.7	-19.3	5.58	-243	-202	-146	41.1	5.47	11.5	16.1	3.93	7.4	0.99
Batagaika River	3	-22.6	-21.3	-20.1	1.8	-175	-164	-152	16.3	5.47	6.82	8.17	1.91	8.9	0.99
Yana River	2	-21.3	-21.3	-21.3	0.01	-162	-162	-162	0.07	8.12	8.13	8.14	0.01	10	1.00
Slump	6	-32.3	-31.5	-30.5	0.57	-243	-237	-233	3.60	11.2	14.6	16.1	1.78	5.9	0.86

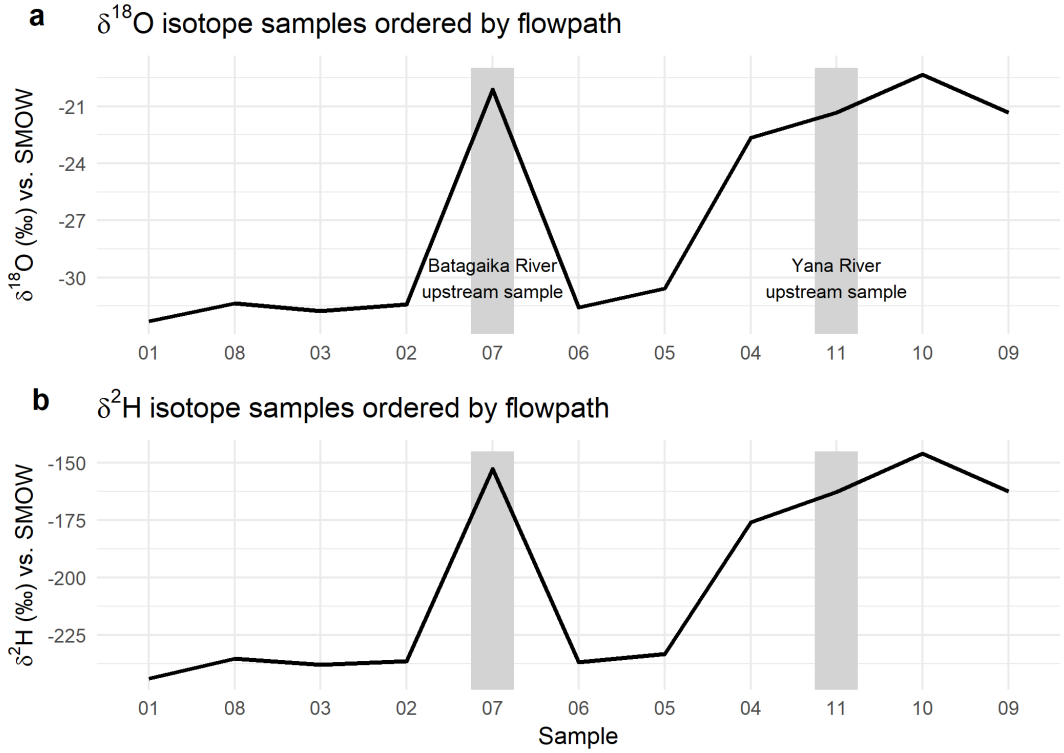

Figure 18 δ^{18}O (a) and δ^{2}H (b) isotope values listed by flow path. The grey columns mark both upstream samples taken, before the slump flows into the Batagaika River and the Batagaika into the Yana River.

4.3 Particulate Organic Matter Characteristics

In general, slump values are the lowest in terms of TC, TIC and TOC, while Batagaika River samples contain the highest values. Batagaika samples show a decrease in TC (6.83 % to 2.09 %), TIC (5.08 % to 1.62 %) and TOC (1.75 % to 0.46 %) moving downstream (Fig. 19; Tab. 3). The highest concentrations occur directly after the slump outflow, although slump samples show much lower concentrations (TC: 0.85 % to 1.08 %, TIC: 0.82 % to 0.92 %, TOC: 0.03 % to 0.15 %). Yana River sample TC values range from 2.25 % to 2.38 %, with 1.88 % of TOC in both samples and 0.36 % to 0.49 % of TIC. Overall TN values are low (0.12 % to 0.52 %) and do not differ clearly between the sample groups (Fig. 19d). Sediment contents of the slump stream water range from 53.2 % to 63.4 %, while Batagaika and Yana River sediment contents are below 2 % (Fig. 19e; Tab. 3). The dry bulk density in the slump ranges

from 1.24 g/cm^3 to 1.54 g/cm^3 (Tab. 3). A dry bulk density of 1.28 g/cm^3 was calculated for the Batagaika River sample before the inflow into the Yana River. The remaining samples did not have enough sediment content to calculate a dry bulk density.

Table 3 Summary of total carbon, total nitrogen, total inorganic carbon, total organic carbon and TOC / TN ratio data.

Sample	TC (%)	TN (%)	TIC (%)	TOC (%)	TOC / TN ratio	dry bulk density (g/cm^3)	sediment content (%)	Description
B17-MF-01	1.06	0.17	0.15	0.91	6.26	1.41	60.1	Slump
B17-MF-02	1.08	0.16	0.15	0.92	6.63	1.28	56.8	Slump
B17-MF-03	0.97	0.14	0.10	0.87	6.86	1.47	63.4	Slump
B17-MF-04	6.02	0.52	1.34	4.67	10.3	-	0.26	Batagaika River
B17-MF-05	6.83	0.47	1.75	5.08	12.4	-	0.43	Batagaika River
B17-MF-06	1.05	0.14	0.14	0.90	7.49	1.54	53.2	Slump Outflow
B17-MF-07	-	-	-	-	-	-	0.15	Batagaika River
B17-MF-08	0.85	0.12	0.03	0.82	7.90	1.24	55.9	Slump
B17-MF-09	2.38	0.22	0.49	1.88	10.1	-	0.15	Yana River
B17-MF-10	2.09	0.23	0.46	1.62	8.22	1.28	1.26	Batagaika River
B17-MF-11	2.25	0.21	0.36	1.88	10.1	-	0.17	Yana River

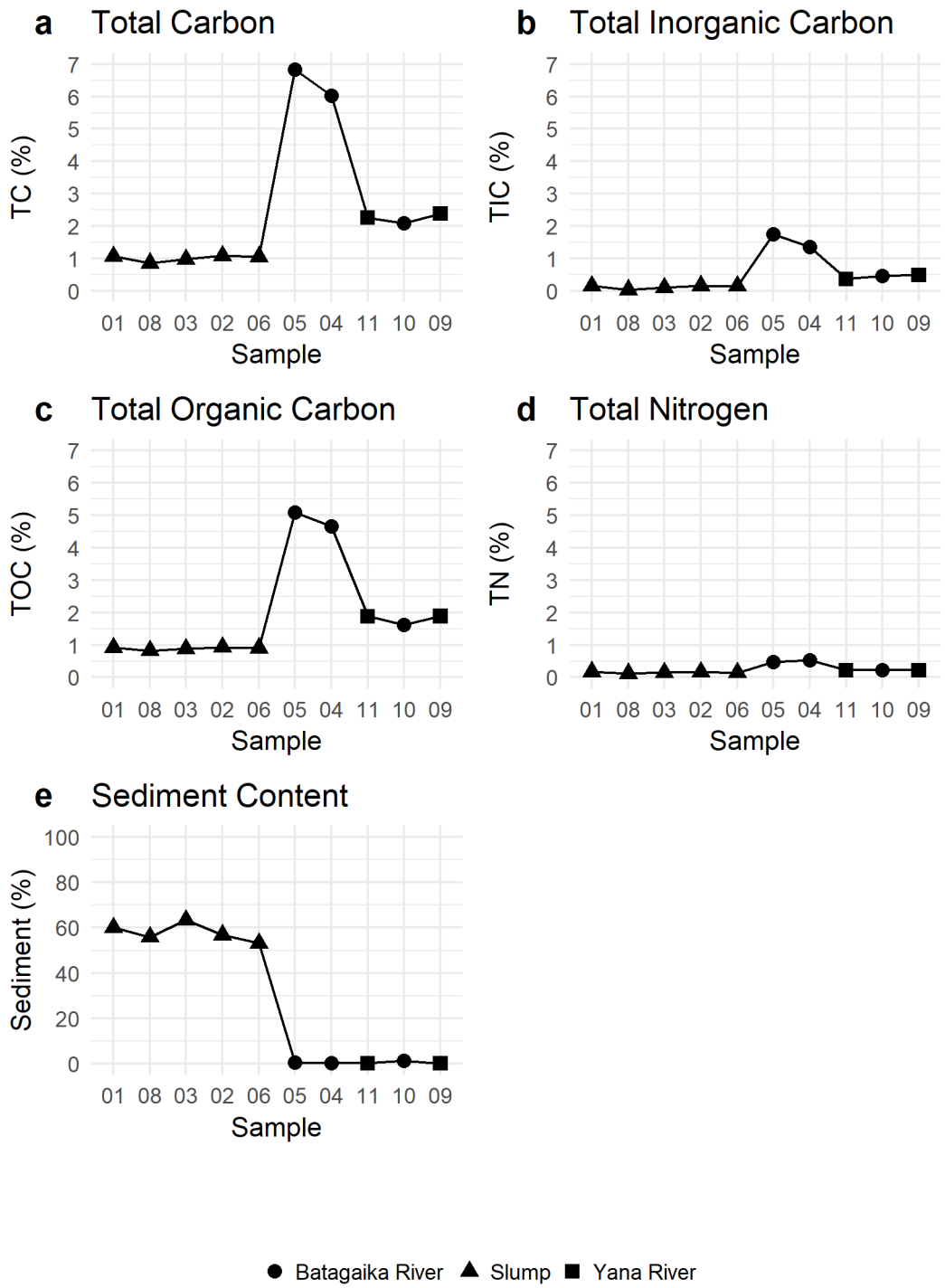

Figure 19 **(a)** Total carbon, **(b)** total inorganic carbon, **(c)** total organic carbon, **(d)** total nitrogen and **(e)** sediment content shape coded by the sample locations Slump, Batagaika and Yana River.

4.3.1 Stable Carbon Isotopes of TOC and DOC and C/N Ratios

δ^{13}C values of TOC are heavier (most negative) than DOC values and are significantly different throughout the flow path (Fig. 20). In the slump the TOC δ^{13}C values range from -24.5 ‰ to -24.1 ‰ decreasing throughout the Batagaika River section with a range of -25.3 ‰ to -24.8 ‰, further to the Yana River with -26.4 ‰ upstream of the Batagaika outflow (-24.8 ‰) and -26.2 ‰ downstream of the inflow. δ^{13}C values of DOC remain in a narrow range from the slump to the Batagaika outflow (-26.3 ‰ to -25.9 ‰). Except for the value of the Batagaika River sample upstream of the slump outflow (-27.3 ‰) the values after the mixing of the slump water with the Batagaika River show only a slight decrease towards the Yana River (Fig. 20). Converging with the Yana River a stronger decrease is shown, as the values drop from -26.3 ‰ from the Batagaika outflow to -27.6 ‰ upstream and -27.5 ‰ downstream of the Yana River.

Slump TOC / TN ratios (6.26 - 7.90) are lower as in the Batagaika (8.22 - 12.4) and Yana (both samples 10.1) (Fig. 21; Tab. 3). DOC / DN ratios are higher than the TOC / TN ratios except for the Batagaika River outflow sample. One DOC / DN slump sample (03) with 20.6 is above the other slump samples including the first Batagaika River sample downstream of the slump outflow, which are in a similar range (15.6 - 16.1). Moving downstream the Batagaika River the DOC / DN values decrease to 9.09 in the Batagaika River outflow. In both DOC and TOC, atomic C/N ratios of the Batagaika River section show a negative gradient with decreasing ratios. However DOC / DN values decrease with a stronger gradient.

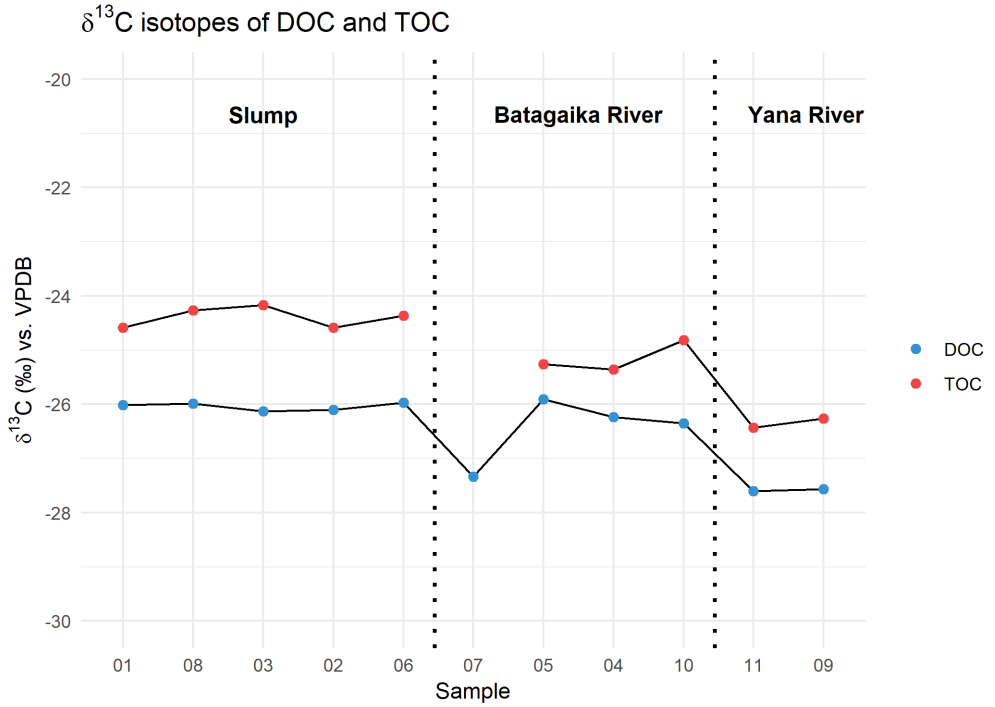

Figure 20 δ^{13}C-DOC and δ^{13}C-TOC isotope data in ‰ vs. VPDB. Subdivided by sample location slump, Batagaika and Yana River.

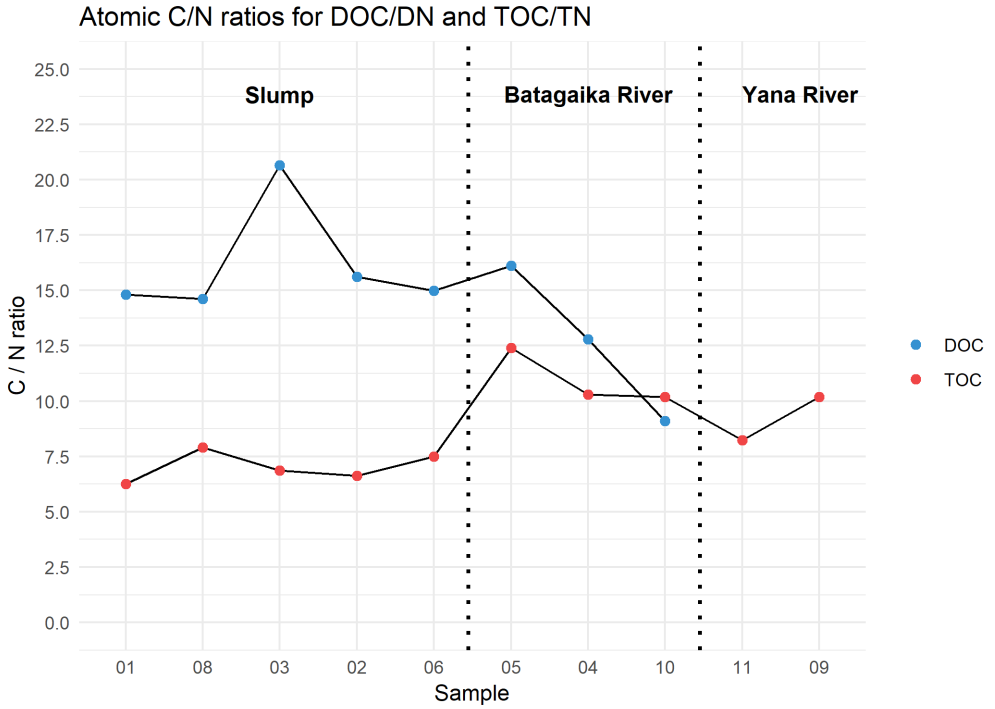

Figure 21 Atomic C/N ratios for DOC/DN and TOC/TN, subdivided by sample locations slump, Batagaika and Yana River.

4.3.2 Radiocarbon Dating Ages of TOC and DOC

AMS ^{14}C σ2 calibrated ages of TOC range from 16.994 ± 0.216 ka BP to 40.861 ± 0.499 ka BP throughout all the data (Tab. **??**). A clear distinction between slump, Batagaika River and Yana River samples is evident. Slump samples range between 33.381 ± 0.347 ka BP and 40.861 ± 0.499 ka BP. Batagaika River samples from 24.185 ± 0.226 ka BP to 31.034 ± 0.183 ka BP and Yana River samples between 16.994 ± 0.261 ka BP and 18.672 ± 0.133 ka BP (Fig. 22).

The ^{14}C-DOC σ2 calibrated ages show a similar pattern, ranging from 0.814 ± 0.109 ka BP to 34.651 ± 0.453 ka BP in the 7 samples which were measured (Tab. 12). Slump sample ages range from 28.036 ± 0.313 ka BP to 34.651 ± 0.453 ka BP, Batagaika River samples from 1.749 ± 0.125 ka BP, in the sample taken upstream of the slump outflow, to 34.444 ± 0.425 ka BP from the sample located 6 km downstream of the slump outflow. Yana River DOC ages range from 0.814 ± 0.109 ka BP to 0.842 ± 0.110 ka BP. Fig. 22 summarizes calibrated radiocarbon ages of ^{14}C-TOC and ^{14}C-DOC. Both datasets indicate a decrease of the sample ages starting from slump samples to Yana River samples.

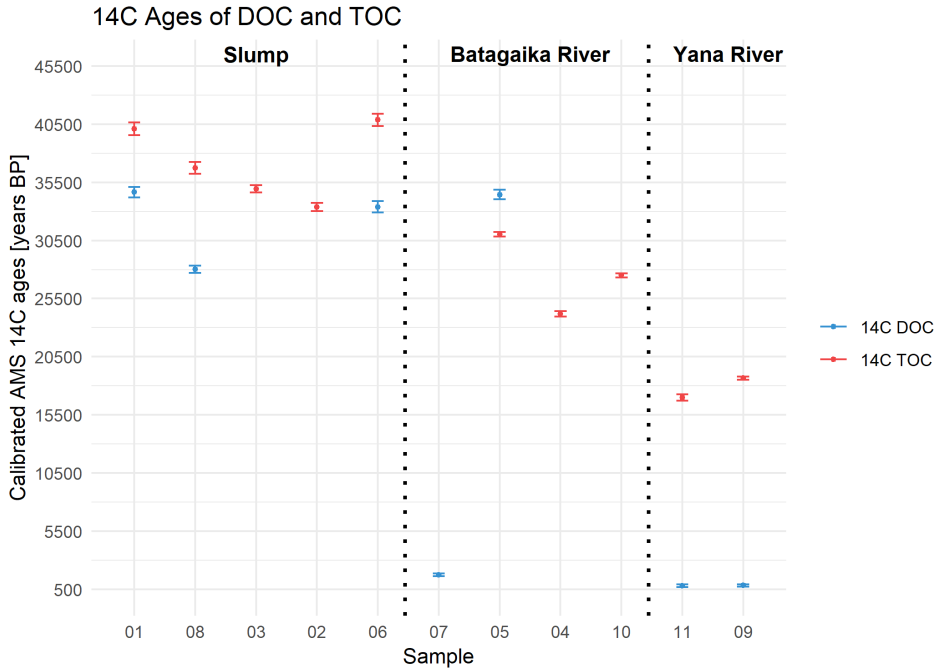

Figure 22 Calibrated AMS ^{14}C ages (2-sigma range, in years BP) of TOC in red and DOC in blue.

4.4 Principal Components

The first two axes of the PCA explain 96.6 % of the variation in the data (Fig. 23). K^+, Cl^-, Na^+, Mg^{2+}, Ca^{2+}, HCO_3^- and SO_4^- ions as well as Si, Fe, DOC, electrical conductivity and d-excess are negatively correlated with the first axis. $\delta^{18}O$ isotopes are positively correlated with the first axis. Positively correlated to the second axis are TN, TC, TIC and TOC. Taking into consideration the sample locations within the PCA biplot, three distinct groups can be distinguished. (1) Slump in the lower left quadrant, (2) Batagaika River in the upper right quadrant and (3) Batagaika outflow and Yana River in the lower right quadrant. With 73.5 % of the variation the first axis probably distinguishes the sample location, taking into consideration the vast domination of variables negatively and $\delta^{18}O$ positively correlating with the first axis showing the decrease of values except for $\delta^{18}O$ where the isotopic composition becomes more positive further downstream.

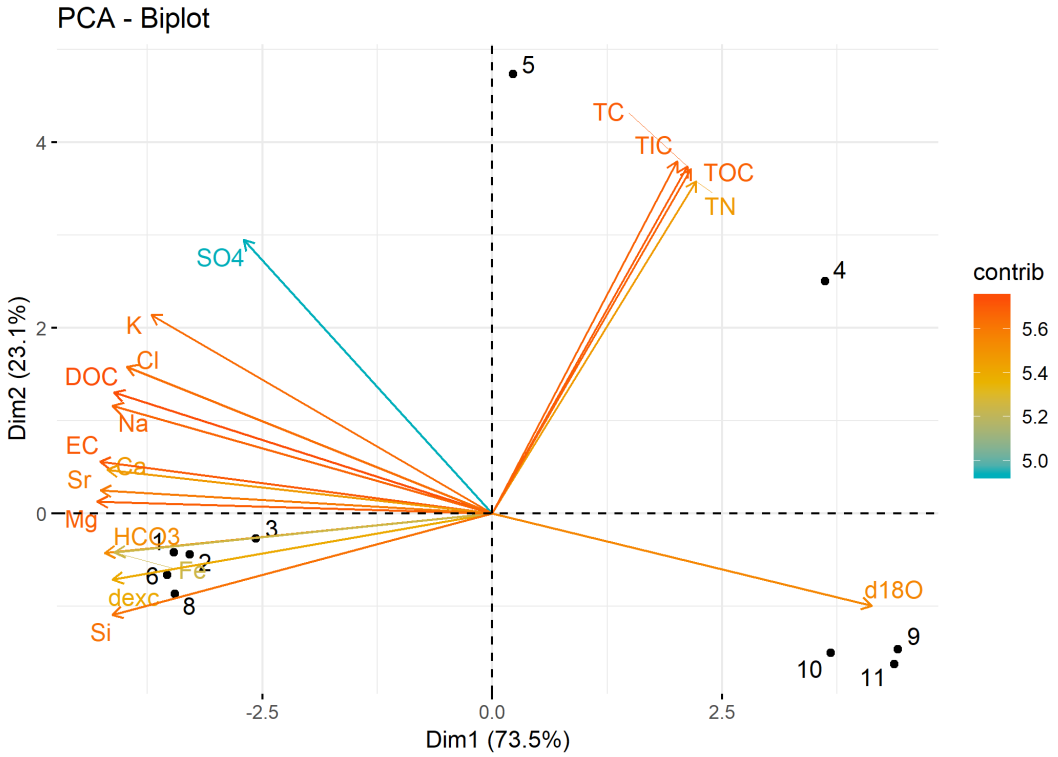

Figure 23 PCA biplot for the dataset color coded by their percentage of contribution to both axes. Individuals represent the sample points.

5 Discussion

5.1 Release and Fate of DOM and DIM from the Slump to the Yana River

A significant release of dissolved organic and inorganic matter was detected due to the permafrost thaw in the Batagay thaw slump. Permafrost slumping has usually been associated with a significant release and increase of DOC from terrestrial to aquatic systems in Eastern Siberia (Spencer et al., 2015) and Alaska (Abbott et al., 2014). In this study DOC release from the slump occurs in high concentrations, while downstream of the slump the DOC concentrations decrease rapidly. This differs from other studies where the DOC release also increases the DOC concentrations downstream (Abbott et al., 2015; Spencer et al., 2015). A study of (Littlefair et al., 2017) described dissolved carbon delivery to streams in the Northwestern Territories in Canada, where DOC release did not affect the downstream concentrations. Degradation of organic matter due to microbiological activity impacts the DOC and DON concentrations indicated by DOC/DON ratios (Fig. 21) (Tanski et al., 2017). The decrease of the ratio from 20 in the slump to 8 in the Batagaika River indicates a higher degree of decomposition of organic matter (White, 2013; Gregorich and Carter, 2007). Additionally, decreasing DOC concentrations downstream of slumps could be driven by DOC sorption to suspended inorganic sediments (Littlefair et al., 2017), dilution due to freshwater supply and possibly due to rapid DOC mineralization. Sorption of DOC can occur in seconds to minutes in freshwater systems (Qualls and Haines, 1992). Radiocarbon ages of ^{14}C-DOC differ clearly from slump or near slump affected water (Pleistocene) and Yana River water as well as upstream Batagaika River water with a late Holocene signal. This provides further evidence that released slump DOC does not reach the Yana River in measurable quantities. The same difference regarding the slump stream water and its impact downstream is shown by δ^{18}O signatures suggesting a strong dilution of the slump signal. Batagaika and Yana River both have a mean value of -21.3 ‰ which lies

in the regional isotopic signal (wateriso.utah.edu/waterisotopes/media/IsoMaps/. Acessed January 7, 2019), while the mean slump value is -31.5 ‰.

In addition to DOC other parameters such as concentrations of major ions, trace and heavy metals experience an increase due to the mobilization of previously frozen sediments. This is in good agreement with other studies showing a high release of major ions due to slumping (Kokelj et al., 2005; Fritz et al., 2015; Houben et al., 2016). High concentrations of major ions also indicate ongoing slumping activity (Littlefair et al., 2017; Fritz et al., 2015). After a significant impact on the ionic composition of the Batagaika River the ion concentrations decrease further downstream and towards the Yana River. The slump clearly affects the Batagaika River, as shown in the piper diagram (Fig. 15). A change in water chemistry due to slumping was also shown by Kokelj et al. (2005) and Houben et al. (2016), who studied the water chemistry of thaw slump affected lakes in the Mackenzie Delta region in Canada. Slump water samples are densely clustered and categorized as water with high hydrogen carbonate content, while Batagaika River samples are more disperse due to the rapid decrease in ionic concentration. The other cluster (Yana River) is categorized as hydrogen carbonatic sulfatic water, both before and after the inflow of the Batgaika River.

The release of ammonium is very high compared to the up- and downstream concentrations, while nitrate release in the slump is very low but increasing on the Batagaika River section (Fig. 13). This could be explained through ongoing nitrification along the flow path, where nitrifying bacteria nitrificate ammonium to nitrite and then further to nitrate (Bothe et al., 2006).

In general, the trend in most parameters is towards a decrease of the initial disturbance, shifting towards a complete dilution originating from the slump due with the mixing of massive ice beds, as well as the Batagaika and Yana River. However, along the Batagaika River other factors besides dilution could be responsible for the decrease in dissolved matter concentrations. Plants needing macro nutrients (N, P, K, S, Ca and Mg) as well as micro nutrients (Co, Cu, Fe, Mn) for growth (Wuana and Okieimen, 2011) and the adsorption of heavy metals in river sediments might explain the decrease of Fe and Zn along the flow path, resulting in concentrations similar to the pre-slump state of the water (Ba, Fe, Si, Cl^-, Na^+ DOC, DN and DON)

or a leveling into the water chemistry of the Yana River without any major impact (Sr, Zn, Mg^{2+}, Ca^{2+}, K^{+}, SO_4^{-} and NH_4^{+}), due to its higher discharge compared to the Batagaika River.

The slump does not seem to affect the Batagaika and Yana River in terms of sediment content. According to Kokelj et al. (2013) sediment material is released to aquatic systems due to permafrost thaw in mega slumps. Sediment contents of the stream water (Fig. 19e) were shown to be over 50 % in the slump but dropping below 2 % in the Batagaika and Yana River. However, Kokelj et al. (2013) described diurnal fluctuations of water levels, solute and sediment flux in the slump impacted streams. This might also be the case in this thesis as sampling occurred while sediment flux was low. Otherwise the generally assumed effect of sediment release to aquatic systems (Kokelj et al., 2013) due to slumping might not apply in this case.

5.2 Dissolved and Particulate Matter

In contrast to the radiocarbon ages of DOC which show a significant difference between slump affected (Pleistocene signal) and unaffected (Holocene signal) water, the radiocarbon ages of TOC from slump to Yana River all show Pleistocene ages. Comparing dissolved and particulate matter from the headwall into the slump DOC (Fig. 11) and DN (Fig. 12) are released in high concentrations, experience a steady decrease as they move towards the Yana River. TOC and TN (Fig. 19) values of the suspended material of the slump are low from the beginning. Due to the waters prolonged contact with the surrounding sediment TOC is potentially subject to leaching and degradation processes and transferred to the DOC pool (Zimov et al., 2006). A very strong correlation between sediment contents and DOC concentrations due to prolonged contact of melt water during segregation within massive ice was shown by Tanski et al. (2016) and Fritz et al. (2015). Leaching of TOC from sediments to the DOC pool is also supported by Artinger et al. (2000) and Dou et al. (2008). Batagaika River TOC values are higher than Slump TOC values but decrease towards the Yana River, while TN values remain low along the whole flow path from the Slump to the Yana River. The abrupt increase of TOC might originate from the upstream section of the Batagaika River itself. The principal component analysis (Fig. 23) confirms a correlation between higher values of TOC, TIC, TN, TN and TC in the Batagaika River section.

The TOC / TN ratio plotted against the δ^{13}C values shows a more aquatic drawn signal (Fig. 24). Especially the slump samples and the Batagaika sample directly after the slump outflow tend to the lacustrine algae signal. Most of the DOC samples, such as the slump samples and the first Batagaika River sample after the slump outflow, are drawn towards the terrestrial C3 plant signal. Towards the Batagaika outflow the DOC / DN ratio decreases (Fig. 21), showing a more lacustrine algae signal. The TOC Batagaika and Yana River samples are also drawn towards the lacustrine algae signal further downstream of the slump (Fig. 24).

C/N ratios of TOC/TN and DOC/DN show an opposite trend (Fig. 21). While DOC/DN ratios remain high after initial slumping and decreasing along the flow path (20 to 8), TOC/TN ratios are low in the slump and experience an increase after initial mixing with the Batagaika River (6 to 12) followed by a decrease to 10 further downstream. Several studies suggest that DOC components contributed from permafrost are more labile and biodegradable than TOC, as DOC was proba-

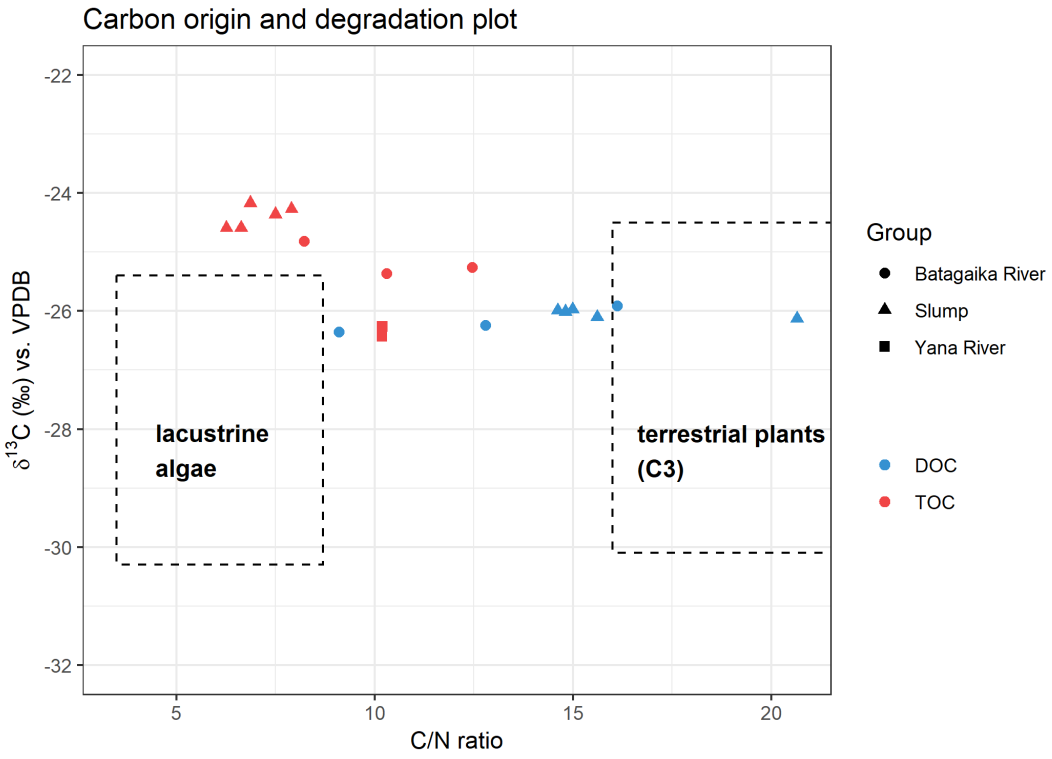

Figure 24 δ^{13}C-DOC and δ^{13}C-TOC isotope data in ‰ vs. VPDB plotted against the atomic C/N ratio. Grouped by the sample locations slump, Batagaika and Yana River. Classification adapted from Meyers (1997)

bly unprocessed before mobilization, consisting of labile, low molecular weight and few aromatic compounds (Dutta et al., 2006; Waldrop et al., 2010). For example, Knoblauch et al. (2013) showed that the highest mineralization rates where found directly after permafrost thaw, and Vonk et al. (2013) showed a loss of up to 33 % of Yedoma OC in 14 days. In this study, however, high DOC/DN ratios and low δ^{13}C-DOC values in the slump suggest little decomposition of DOC directly after permafrost thaw. The low TOC/TN ratios are unusual for Yedoma deposits as the OC in Yedoma deposits is regarded as readily available carbon (Strauss et al., 2013; Zimov et al., 2006) The higher degree of decomposition for TOC in the slump might be due to longer residency and exposure to microbiological activity of particulate matter than dissolved matter. Ward et al. (2017) suggest that the initial low degradation of DOC is potentially caused by the photo-degradation of DOC compounds due to sunlight exposure, which microbiological communities from permafrost soils are not metabolically equipped to consume. Further downstream the photo-altered smaller, aliphatic and less oxidized DOC compounds encounter the more adapted microbiological communities for mineralization (Ward et al., 2017). However, this might not be the case according to Vonk et al. (2013), who concluded that DOC in Yedoma ice wedges can be regarded as readily available carbon source with high content of low molecular weight compounds. The increase of the TOC/TN ratio from the slump to the Batagaika River could be subject to the absorption to mineral particles and thus be protected by organo-mineral bonds from microbiological degradation (Höfle et al., 2013; Huguet et al., 2008; Keil et al., 1994). Otherwise, the ratio should decrease more as the supply of TOC and TN increases slightly in the Batagaika River, while actually providing more nutrients for microorganisms.

5.3 Relating Slump Material to Stratigraphical Slump Headwall Units

The stable water isotopes slump stream water samples have a mean δ^{18}O value of -31.5 ‰ and d-excess of 14.6 ‰, which is in good agreement with slump outflow water samples from Opel et al. (2018) (mean δ^{18}O of -31.7 ‰ and d-excess of 15.2 ‰). In relation to the stratigraphy of the headwall, ice wedges of the upper sand (Unit II) with mean δ^{18}O values of -31.8 ‰ and -32.8 ‰, and mean d-excess values of 14.7 ‰ and 15.1 ‰ (Opel et al., 2018) could be a major part of the melt water source. The intrasedimentary ice of the upper sand (Unit II) shows a similar mean δ^{18}O value

Table 4 Summary of the biogeochemical parameters of this study at the NNE slump headwall and data from Ashastina et al. (2017b) close to the same location. Data is grouped according to cryostratigraphical units in Ashastina et al. (2017b) and compared to suspended slump surface water material.

Sample Location	TC		TN		TIC		TOC		TOC / TN		δ^{13}C-TOC	
	(%)	sd	(%)	sd	(%)	sd	(%)	sd	ratio	sd	(‰)	sd
Unit I/A	0.30	0.02	0.12	-	0.31	0.04	< 0.10	-	-	-	-	-
Unit II/A	1.31	0.71	0.19	0.06	0.29	0.08	1.22	0.63	4.82	1.19	-24.7	0.28
Unit III/B	3.62	0.04	0.26	-	0.31	0.03	3.31	0.01	10.9	0.03	-26.3	0.25
Slump sample 01	1.06	-	0.17	-	0.15	-	0.91	-	6.26	-	-24.5	-
Slump sample 08	0.85	-	0.12	-	0.03	-	0.82	-	7.90	-	-24.2	-

(-30.5 ‰), however with a mean d-excess value of 24.4 ‰. Intrasedimentary ice of the lower sand (Unit V) (mean δ^{18}O of -32.3 ‰ and d-excess of 14.7) is also in good agreement with slump water values. According to this data, slump waters might originate from ice wedges of the upper sand (Unit II) and intrasedimentary ice of the lower sand (Unit V). That stated, the slump water might contain more ice wedge than instrasedimentary melt water due to the larger volume of the ice wedges. Ice wedge δ^{18}O values of the upper ice complex (Unit III) are around -35 ‰ (Opel et al., 2018). Ice wedges from the upper ice complex studied by Vasil'chuk et al. (2017) show similar δ^{18}O values (Tab. 10).

Other parameters such as TC, TN, TIC, TOC, TOC/TN and δ^{13}C from the suspended slump material show a correspondence to the upper sand (Unit II) of the NNE headwall when compared with Ashastina et al. (2017b) data. For example, sample point 01, which is part of the drainage section of the NNE headwall, and sample point 08 further downstream and part of the slump main drainage (Tab. 4). In general, the other suspended slump material samples also relate to the upper sand (Unit II) TC, TN, TIC, TOC, TOC/TN and δ^{13}C data from Ashastina et al. (2017b).

AMS ^{14}C-TOC slump values range from 33 ka BP and 40 ka BP (Tab. **??**), and partially fit into the dating results of Ashastina et al. (2017b), which correspond to Unit II. Plant remains of Unit II were 2σ calibrated and dated 37 - 38 ka BP, ground squirrel droppings 28 - 29 ka BP and plant remains of a section SE of the headwall

corresponding to Unit III with 15 ka BP and 52 ka BP. Radiocarbon ages obtained by Murton et al. (2017) from Unit II on the NNE headwall shows a similar range with 37 - 40 ka BP as slump sample 01 with 39 - 40 ka BP. Sediment dating results from Opel et al. (2018) show an age range of 42 - 43 ka BP in Unit II and > 50 ka BP in Unit III, both from the SE section of the headwall. However, slump stream sediment dating (33 to 41 ka BP) represents ages with a better fit to the NNE part of the headwall, where ages range from 28 to 40 ka BP in Unit II. This includes slump stream sediments located towards the slump outflow, where the sediment of the whole slump should accumulate. The absence of younger material at the slump outflow suggests that, above all, material from the NNE headwall of Unit II is transported there. For otherwise, signals of ^{14}C-TOC ages between 12 ka BP and 28 ka BP would be among the slump samples. However, Ashastina et al. (2017b) describe the southwestern part of the slump headwall as most actively eroding; therefore, material from that part of the headwall should also be transported outwards of the slump. Moreover, the absence of non-finite ^{14}C ages in all slump samples in this study is unusual as also the lower units erode and were dated by Ashastina et al. (2017b) to > 100 ka BP with OSL and IRSL. This might be explained by the internal transport and deposition dynamics of sediments within the slump or simply the lack of a higher sampling resolution of both the headwall sections and slump streams.

6 Conclusion

This study of the Batagaika thaw slump in central Yakutia, Russia, provides data about the release of dissolved and particulate organic and inorganic matter and their impact on downstream rivers. Stable isotope data and radiocarbon dating reflect the erosion origin from the slump headwall units to slump surface streams. The following results can be concluded:

- Permafrost thaw at the Batgaika thaw slump releases huge amounts of organic and inorganic dissolved matter into the downstream ecosystems (**DOC:** 172 mg/l, **DON:** 9.74 mg/l, **Mg^{2+}:** 159 mg/l, **$Ca:^{2+}$:** 178 mg/l, **Na^{+}:** 88.8 mg/l, **K^{+}:** 5.38 mg/l, **Cl^{-}:** 66.8 mg/l and **$SO_4{}^{2-}$:** 113 mg/l at the slump outflow). The data shows a general trend of decreasing concentrations of the solutes once the slump waters flow into the Batagaika River and further into the Yana River. The Yana River water chemistry shows no significant change due to slumping and thus might not be affected by it, while the Batagaika River is clearly affected by the slump comparing water chemistry before and after the slump water inflow. As mentioned, the solute concentrations decrease over the 5-6 km of the Batagaika River section to nearly the values they had before mixing with the slump water, self-regulating the disturbance.

- Particulate matter from the slump does not seem to have an affect on the Batagaika and Yana River as TC, TOC and TIC values of the slump are clearly lower than Batagaika River values. Untypical for Yedoma deposits are the low TOC/TN ratios found in the slump samples, implicating a high degree of decomposition although Yedoma carbon is regarded as mostly undecomposed carbon (Zimov et al., 2006). As mentioned, the longer residency and exposure of TOC to microbiological activity of particulate matter than dissolved matter might explain these results in this study. Sediment content of the samples were >50 % in the slump and dropped to <2 % in the Batagaika and Yana River, suggesting that the slumping might not have a strong impact in terms of sediment release and transport to downstream ecosystems. Although sediment

transport from the slump to subsequent aquatic systems must happen due to fluvial transport, the observed impact of dissolved matter to the Batagaika and Yana River is significantly stronger.

- Comparing the slump stream data with the slump headwall data from other studies showed that the melt water source of the slump stream can be related to the ice wedges of the upper sand (Unit II) and intrasedimentary ice of the lower sand (Unit V), with possibly higher content of melt water from the upper sand ice wedges due to their larger volume. Particulate matter in the slump stream shows a similarity with values of the upper sand (Unit II) of the NNE section of the headwall. This suggests a major erosion of the upper sand unit at that time. Erosion of the Batagaika thaw slumps headwall, however, had to occur in every unit while forming and growing over the last 40 years. Especially the absence of non-finite radiocarbon ages in the slump samples in this study leave an uncertainty regarding erosional dynamics. Data from Murton et al. (2017), Ashastina et al. (2017b) and Opel et al. (2018) show non-finite radiocarbon ages and ages dated with OSL and IRSL $>$ 100 ka BP from lower units (Ashastina et al., 2017b). Erosional dynamics might change over certain periods of time connected to the erosional state of the individual units, leading to a shift of the erosion source and thus an overall advance of the headwall.

6.1 Outlook

Results of this thesis are based on a one time sampling. For future studies a field campaign with sampling of the same locations over time might show different results and present diurnal dynamics or effects on a larger scale, which could affect the input of the slump water and suspended material into the Batagaika and Yana River. Spatially consistent sampling of the whole slump could reveal inner dynamics of the drainage system regarding the erosion and sediment transport of headwall material. In addition, the sampling of more than one location before the inflow of the slump into the Batagaika River might help explain the water chemistry and dynamics of the Batagaika River in its undisturbed and subsequent disturbed phase. On a global scale the Batagaika thaw slump is contributing to climate change with its release of huge amounts of DOC and subsequent microbiological breakdown to CO_2. Calculating solute fluxes such as DOC could contribute to estimate and model

carbon losses, due to permafrost thaw, as well as estimate future erosion rates of the thaw slump. Future projected Arctic warming may lead to increasing headwall ablation of the slump, along with further release of dissolved and particulate matter that was previously stored in permafrost. Furthermore, the Batgaika thaw slump's ongoing erosion would also affect the surrounding landscape and surface vegetation. This involves deforestation, which leads to a negative impact on the surface capacity of storing atmospheric carbon with photosynthesis.

Acknowledgements

I would like to thank my supervisor Dr. Michael Fritz and the COPER group at the Alfred-Wegener-Institute in Potsdam for giving me the opportunity to work on an interesting and challenging master thesis. Thanks to Thomas Opel and Ksenia Ashastina, who took the samples I could work on.

Special thanks to Dyke Scheidemann and Antje Eulenburg for instructing and helping me with the lab work and preparation of the samples. Christian Knoblauch at the University of Hamburg for measuring dissolved carbon and nitrogen compounds. Janet Rethemeyer at the University of Cologne for DOC radiocarbon dating. Gesine Mollenhauer at the Alfred-Wegener-Institute in Bremerhaven for radiocarbon dating of particulate organic carbon. Juliane Wolter who helped me with RStudio related challenges and Thomas Opel for consultation on the Batagaika thaw slump site and interpretation of the data. And to apl. Prof. Dr. Dieckmann at the University of Potsdam and the Alfred-Wegener-Institute in Potsdam for reviewing this thesis. Big thanks again to Michael Fritz for his supervision and for helping me come up with new interpretations, as well as and giving me new insights of the process of conducting scientific work.

I would also like to thank all of my friends and my family, who always supported me throughout all my years of study.

Bibliography

Abbott, B. W., Jones, J. B., Godsey, S. E., Larouche, J. R., and Bowden, W. B. (2015). Patterns and persistence of hydrologic carbon and nutrient export from collapsing upland permafrost. *Biogeosciences*, 12(12):3725–3740.

Abbott, B. W., Larouche, J. R., Jones, J. B., Bowden, W. B., and Balser, A. W. (2014). Elevated dissolved organic carbon biodegradability from thawing and collapsing permafrost. *Journal of Geophysical Research: Biogeosciences*, 119(10):2049–2063.

Artinger, R., Buckau, G., Geyer, S., Fritz, P., Wolf, M., and Kim, J. (2000). Characterization of groundwater humic substances: influence of sedimentary organic carbon. *Applied Geochemistry*, 15(1):97–116.

Ashastina, K., Kienast, F., Römermann, C., Kuzmina, S., Diekmann, B., and Schirrmeister, L. (2017a). The Batagay permafrost mega thaw slump: an environmental archive of the late Pleistocene continental climate. In *EGU General Assembly Conference Abstracts*, volume 19, page 959.

Ashastina, K., Schirrmeister, L., Fuchs, M., and Kienast, F. (2017b). Palaeoclimate characteristics in interior Siberia of MIS 6–2: first insights from the Batagay permafrost mega-thaw slump in the Yana Highlands. *Climate of the Past*, 13(7):795.

Auguie, B. (2017). *gridExtra: Miscellaneous Functions for "Grid" Graphics*. R package version 2.3.

Bernoux, M., Cerri, C. C., Neill, C., and de Moraes, J. F. (1998). The use of stable carbon isotopes for estimating soil organic matter turnover rates. *Geoderma*, 82(1-3):43–58.

Boessenkool, B. (2017). *berryFunctions: Function Collection Related to Plotting and Hydrology*. R package version 1.16.3.

Boike, J., Langer, M., Lantuit, H., Muster, S., Roth, K., Sachs, T., Overduin, P., Westermann, S., and McGuire, A. D. (2012). Permafrost–physical aspects, carbon cycling, databases and uncertainties. In *Recarbonization of the Biosphere*, pages 159–185. Springer.

Bothe, H., Ferguson, S., and Newton, W. E. (2006). *Biology of the nitrogen cycle*. Elsevier.

Brown, J., Ferrians Jr, O., Heginbottom, J., and Melnikov, E. (1997). *Circum-Arctic map of permafrost and ground-ice conditions*. US Geological Survey Reston.

Brown, J., Ferrians Jr, O., Heginbottom, J., and Melnikov, E. (2002). *National Snow and Ice Data Center [WWW Document]. Circum-Arct. Map Permafr. Ground-Ice Cond. Version 2. Accessed October 24, 2018*.

Cheng, G. and Wu, T. (2007). Responses of permafrost to climate change and their environmental significance, Qinghai-Tibet Plateau. *Journal of Geophysical Research: Earth Surface*, 112(F2).

Collins, M., Knutti, R., Arblaster, J., Dufresne, J.-L., Fichefet, T., Friedlingstein, P., Gao, X., Gutowski, W., Johns, T., Krinner, G., et al. (2013). Long-term climate change: projections, commitments and irreversibility.

Craig, H. (1961). Isotopic variations in meteoric waters. *Science*, 133(3465):1702–1703.

Cray, H. A. and Pollard, W. H. (2015). Vegetation recovery patterns following permafrost disturbance in a low Arctic setting: case study of Herschel Island, Yukon, Canada. *Arctic, antarctic, and alpine research*, 47(1):99–113.

Dansgaard, W. (1964). Stable isotopes in precipitation. *Tellus*, 16(4):436–468.

De Hoffmann, E. and Stroobant, V. (2007). *Mass spectrometry: principles and applications*. John Wiley & Sons.

Dou, F., Ping, C.-L., Guo, L., and Jorgenson, T. (2008). Estimating the impact of seawater on the production of soil water-extractable organic carbon during coastal erosion. *Journal of environmental quality*, 37(6):2368–2374.

Dutta, K., Schuur, E., Neff, J., and Zimov, S. (2006). Potential carbon release from permafrost soils of Northeastern Siberia. *Global Change Biology*, 12(12):2336–2351.

Fritz, M., Opel, T., Tanski, G., Herzschuh, U., Meyer, H., Eulenburg, A., and Lantuit, H. (2015). Dissolved organic carbon (DOC) in Arctic ground ice. *The Cryosphere*, 9:737–752.

Gonfiantini, R., Stichler, W., and Rozanski, K. (1995). Standards and intercomparison materials distributed by the International Atomic Energy Agency for stable isotope measurements. Technical report.

Gregorich, E. G. and Carter, M. R. (2007). *Soil sampling and methods of analysis*. CRC Press.

Günther, F., Grosse, G., Wetterich, S., Jones, B. M., Kunitsky, V. V., Kienast, F., and Schirrmeister, L. (2015). The Batagay mega thaw slump, Yana Uplands, Yakutia, Russia: permafrost thaw dynamics on decadal time scale. TERRA NOSTRA-Schriften der GeoUnion Alfred-Wegener-Stiftung.

Höfle, S., Rethemeyer, J., Mueller, C., and John, S. (2013). Organic matter composition and stabilization in a polygonal tundra soil of the Lena Delta. *Biogeosciences*, 10(5):3145–3158.

Houben, A. J., French, T. D., Kokelj, S. V., Wang, X., Smol, J. P., and Blais, J. M. (2016). The impacts of permafrost thaw slump events on limnological variables in upland tundra lakes, Mackenzie Delta region. *Fundamental and Applied Limnology/Archiv für Hydrobiologie*, 189(1):11–35.

Hugelius, G., Strauss, J., Zubrzycki, S., Harden, J. W., Schuur, E., Ping, C.-L., Schirrmeister, L., Grosse, G., Michaelson, G. J., Koven, C. D., et al. (2014). Estimated stocks of circumpolar permafrost carbon with quantified uncertainty ranges and identified data gaps. *Biogeosciences Discussions*, 11.

Huguet, C., de Lange, G. J., Gustafsson, Ö., Middelburg, J. J., Damsté, J. S. S., and Schouten, S. (2008). Selective preservation of soil organic matter in oxidized marine sediments (Madeira Abyssal Plain). *Geochimica et Cosmochimica Acta*, 72(24):6061–6068.

IPCC (2013). *Climate Change 2013: The Physical Science Basis. Contribution of Working Group I to the Fifth Assessment Report of the Intergovernmental Panel on Climate Change*. Cambridge University Press, Cambridge, United Kingdom and New York, NY, USA.

Ivanova (2006). Record low air temperatures of Eurasia, (in russian). 3:13–19.

Jolliffe, I. (2011). Principal component analysis. In *International encyclopedia of statistical science*, pages 1094–1096. Springer.

Jorgenson, M. T., Shur, Y. L., and Pullman, E. R. (2006). Abrupt increase in permafrost degradation in Arctic Alaska. *Geophysical Research Letters*, 33(2).

Kassambara, A. and Mundt, F. (2017). *factoextra: Extract and Visualize the Results of Multivariate Data Analyses*. R package version 1.0.5.

Keil, R. G., Montluçon, D. B., Prahl, F. G., and Hedges, J. I. (1994). Sorptive preservation of labile organic matter in marine sediments. *Nature*, 370(6490):549.

Keuper, F., Van Bodegom, P. M., Dorrepaal, E., Weedon, J. T., Van Hal, J., Van Logtestijn, R. S., and Aerts, R. (2012). A frozen feast: Thawing permafrost increases plant-available nitrogen in subarctic peatlands. *Global Change Biology*, 18(6):1998–2007.

Knoblauch, C., Beer, C., Sosnin, A., Wagner, D., and Pfeiffer, E.-M. (2013). Predicting long-term carbon mineralization and trace gas production from thawing permafrost of Northeast Siberia. *Global change biology*, 19(4):1160–1172.

Kokelj, S., Jenkins, R., Milburn, D., Burn, C. R., and Snow, N. (2005). The influence of thermokarst disturbance on the water quality of small upland lakes, Mackenzie Delta region, Northwest Territories, Canada. *Permafrost and Periglacial Processes*, 16(4):343–353.

Kokelj, S., Lacelle, D., Lantz, T., Tunnicliffe, J., Malone, L., Clark, I., and Chin, K. (2013). Thawing of massive ground ice in mega slumps drives increases in stream sediment and solute flux across a range of watershed scales. *Journal of Geophysical Research: Earth Surface*, 118(2):681–692.

Köppen, W. (1884). Die Wärmezonen der Erde, nach der Dauer der heissen, gemässigten und kalten Zeit und nach der Wirkung der Wärme auf die organische Welt betrachtet. *Meteorologische Zeitschrift*, 1(21):5–226.

Kunitsky, V., Syromyatnikov, I., Schirrmeister, L., Skachov, Y. B., Grosse, G., Wetterich, S., and Grigoriev, M. (2013). Ice-rich permafrost and thermal denudation in the Batagay area (Yana Upland, East Siberia). *Earth Cryosphere (Kriosfera Zemli)*, 17(1):56–58.

Lantuit, H. and Pollard, W. (2005). Temporal stereophotogrammetric analysis of retrogressive thaw slumps on Herschel Island, Yukon Territory. *Natural Hazards and Earth System Science*, 5(3):413–423.

Lantuit, H., Pollard, W., Couture, N., Fritz, M., Schirrmeister, L., Meyer, H., and Hubberten, H.-W. (2012). Modern and late Holocene retrogressive thaw slump activity on the Yukon coastal plain and Herschel Island, Yukon Territory, Canada. *Permafrost and Periglacial Processes*, 23(1):39–51.

Lê, S., Josse, J., and Husson, F. (2008). FactoMineR: A Package for Multivariate Analysis. *Journal of Statistical Software*, 25(1):1–18.

Lewkowicz, A. G. (1986). Rate of short-term ablation of exposed ground ice, Banks Island, Northwest Territories, Canada. *Journal of Glaciology*, 32(112):511–519.

Lewkowicz, A. G. (1987). Headwall retreat of ground-ice slumps, Banks Island, Northwest Territories. *Canadian Journal of Earth Sciences*, 24(6):1077–1085.

Littlefair, C. A., Tank, S. E., and Kokelj, S. V. (2017). Retrogressive thaw slumps temper dissolved organic carbon delivery to streams of the Peel Plateau, NWT, Canada. *Biogeosciences*, 14(23):5487–5505.

Lydolph, P. E. (1985). *The climate of the earth*. Government Institutes.

Malone, L., Lacelle, D., Kokelj, S., and Clark, I. D. (2013). Impacts of hillslope thaw slumps on the geochemistry of permafrost catchments (Stony Creek watershed, NWT, Canada). *Chemical Geology*, 356:38–49.

Meyer, H., Schirrmeister, L., Andreev, A., Wagner, D., Hubberten, H.-W., Yoshikawa, K., Bobrov, A., Wetterich, S., Opel, T., Kandiano, E., et al. (2010). Lateglacial and Holocene isotopic and environmental history of northern coastal Alaska–Results from a buried ice-wedge system at Barrow. *Quaternary Science Reviews*, 29(27):3720–3735.

Meyers, P. A. (1997). Organic geochemical proxies of paleoceanographic, paleolimnologic, and paleoclimatic processes. *Organic geochemistry*, 27(5-6):213–250.

Moquin, P. A., Mesquita, P. S., Wrona, F. J., and Prowse, T. D. (2014). Responses of benthic invertebrate communities to shoreline retrogressive thaw slumps in Arctic upland lakes. *Freshwater Science*, 33(4):1108–1118.

Murton, J. B., Edwards, M. E., Lozhkin, A. V., Anderson, P. M., Savvinov, G. N., Bakulina, N., Bondarenko, O. V., Cherepanova, M. V., Danilov, P. P., Boeskorov, V., et al. (2017). Preliminary paleoenvironmental analysis of permafrost deposits at Batagaika megaslump, Yana Uplands, northeast Siberia. *Quaternary Research*, 87(2):314–330.

Nelson, F. E., Anisimov, O. A., and Shiklomanov, N. I. (2001). Subsidence risk from thawing permafrost. *Nature*, 410(6831):889.

Olefeldt, D., Goswami, S., Grosse, G., Hayes, D., Hugelius, G., Kuhry, P., McGuire, A. D., Romanovsky, V., Sannel, A. B. K., Schuur, E., et al. (2016). Circumpolar distribution and carbon storage of thermokarst landscapes. *Nature communications*, 7:13043.

Opel, T., Murton, J. B., Wetterich, S., Meyer, H., Ashastina, K., Günther, F., Grotheer, H., Mollenhauer, G., Danilov, P. P., Boeskorov, V., Savvinov, G. N., and Schirrmeister, L. (2018). Middle and late Pleistocene climate and continentality inferred from ice wedges at Batagay megaslump in the Northern Hemisphere's most continental region, Yana Highlands, interior Yakutia. *Climate of the Past Discussions*, 2018:1–32.

Piper, A. M. (1944). A graphic procedure in the geochemical interpretation of water-analyses. *Eos, Transactions American Geophysical Union*, 25(6):914–928.

Qualls, R. and Haines, B. L. (1992). Measuring adsorption isotherms using continuous, unsaturated flow through intact soil cores. *Soil Science Society of America Journal*, 56(2):456–460.

R Core Team (2013). *R: A Language and Environment for Statistical Computing*. R Foundation for Statistical Computing, Vienna, Austria.

R Core Team (2017). *R: A Language and Environment for Statistical Computing*. R Foundation for Statistical Computing, Vienna, Austria.

Reimer, P. J., Bard, E., Bayliss, A., Beck, J. W., Blackwell, P. G., Ramsey, C. B., Buck, C. E., Cheng, H., Edwards, R. L., Friedrich, M., et al. (2013). IntCal13 and Marine13 radiocarbon age calibration curves 0–50,000 years cal BP. *Radiocarbon*, 55(4):1869–1887.

Romanovsky, V., Drozdov, D., Oberman, N., Malkova, G., Kholodov, A., Marchenko, S., Moskalenko, N., Sergeev, D., Ukraintseva, N., Abramov, A., et al. (2010a). Thermal state of permafrost in Russia. *Permafrost and Periglacial Processes*, 21(2):136–155.

Romanovsky, V. E., Smith, S. L., and Christiansen, H. H. (2010b). Permafrost thermal state in the polar Northern Hemisphere during the international polar year 2007–2009: a synthesis. *Permafrost and Periglacial processes*, 21(2):106–116.

Schaefer, K., Lantuit, H., Romanovsky, V. E., Schuur, E. A., and Witt, R. (2014). The impact of the permafrost carbon feedback on global climate. *Environmental Research Letters*, 9(8):085003.

Schirrmeister, L., Siegert, C., Kuznetsova, T., Kuzmina, S., Andreev, A., Kienast, F., Meyer, H., and Bobrov, A. (2002). Paleoenvironmental and paleoclimatic records from permafrost deposits in the Arctic region of Northern Siberia. *Quaternary International*, 89(1):97–118.

Schuur, E. A., Bockheim, J., Canadell, J. G., Euskirchen, E., Field, C. B., Goryachkin, S. V., Hagemann, S., Kuhry, P., Lafleur, P. M., Lee, H., et al. (2008). Vulnerability of permafrost carbon to climate change: Implications for the global carbon cycle. *AIBS Bulletin*, 58(8):701–714.

Schuur, E. A. G., McGuire, A. D., Schädel, C., Grosse, G., Harden, J. W., Hayes, D. J., Hugelius, G., Koven, C. D., Kuhry, P., Lawrence, D. M., Natali, S. M., Olefeldt, D., Romanovsky, V. E., Schaefer, K., Turetsky, M. R., Treat, C. C., and Vonk, J. E. (2015). Climate change and the permafrost carbon feedback. *Nature*, 520:171 EP –. Review Article.

Shur, Y., Hinkel, K. M., and Nelson, F. E. (2005). The transient layer: implications for geocryology and climate-change science. *Permafrost and Periglacial Processes*, 16(1):5–17.

Slagoda (1991). Microstructure of permafrost slope deposits of the Kisilyakh Range, in: Melnikov, P.I. and Popov, A.I. (eds), Denudation in the cryolithozone. pages 19–29.

Smith, S. L. and Riseborough, D. W. (2010). Modelling the thermal response of permafrost terrain to right-of-way disturbance and climate warming. *Cold Regions Science and Technology*, 60(1):92–103.

Spencer, R. G., Mann, P. J., Dittmar, T., Eglinton, T. I., McIntyre, C., Holmes, R. M., Zimov, N., and Stubbins, A. (2015). Detecting the signature of permafrost thaw in Arctic rivers. *Geophysical Research Letters*, 42(8):2830–2835.

Strauss, J., Schirrmeister, L., Grosse, G., Wetterich, S., Ulrich, M., Herzschuh, U., and Hubberten, H.-W. (2013). The deep permafrost carbon pool of the Yedoma region in Siberia and Alaska. *Geophysical Research Letters*, 40(23):6165–6170.

Stuiver, M. and Reimer, P. J. (1993). Extended 14 C data base and revised CALIB 3.0 14 C age calibration program. *Radiocarbon*, 35(1):215–230.

Tanski, G., Couture, N., Lantuit, H., Eulenburg, A., and Fritz, M. (2016). Eroding permafrost coasts release low amounts of dissolved organic carbon (DOC) from ground ice into the nearshore zone of the Arctic Ocean. *Global Biogeochemical Cycles*, 30(7):1054–1068.

Tanski, G., Lantuit, H., Ruttor, S., Knoblauch, C., Radosavljevic, B., Strauss, J., Wolter, J., Irrgang, A. M., Ramage, J., and Fritz, M. (2017). Transformation of terrestrial organic matter along thermokarst-affected permafrost coasts in the Arctic. *Science of the Total Environment*, 581:434–447.

Van Everdingen, R. (2005). Multi-language glossary of permafrost and related ground-ice terms. National Snow and Ice Data Center/World Data Center for Glaciology, Boulder, CO. *World Wide Web Address: http://nsidc.org/fgdc/glossary*.

Vasil'chuk, Y., Vasil'chuk, J., Budantseva, N., Vasil'chuk, A., and Trishin, A. (2017). Isotopic and geochemical features of the Batagaika Yedoma (preliminary results). *Arctic and Antarctic*, (3):69–96.

Vaughan, D., Comiso, J., Allison, I., Carrasco, J., Kaser, G., Kwok, R., Mote, P., Murray, T., Paul, F., Ren, J., Rignot, E., Solomina, O., Steffen, K., and Zhang, T. (2013). *Observations: Cryosphere*, book section 4, page 317–382. Cambridge University Press, Cambridge, United Kingdom and New York, NY, USA.

Vdovina (2002). *Geological map of Russian Federation*. VSEGEI publishing house.

Vonk, J. E., Mann, P. J., Davydov, S., Davydova, A., Spencer, R. G., Schade, J., Sobczak, W. V., Zimov, N., Zimov, S., Bulygina, E., et al. (2013). High biolability of ancient permafrost carbon upon thaw. *Geophysical Research Letters*, 40(11):2689–2693.

Waldrop, M. P., Wickland, K. P., White Iii, R., Berhe, A. A., Harden, J. W., and Romanovsky, V. E. (2010). Molecular investigations into a globally important carbon pool: Permafrost-protected carbon in Alaskan soils. *Global change biology*, 16(9):2543–2554.

Ward, C. P., Nalven, S. G., Crump, B. C., Kling, G. W., and Cory, R. M. (2017). Photochemical alteration of organic carbon draining permafrost soils shifts microbial metabolic pathways and stimulates respiration. *Nature communications*, 8(1):772.

Werner, R. (2003). The online 18o/16o analysis: development and application. *Isotopes in Environmental and Health Studies*, 39(2):85–104.

White, R. E. (2013). *Principles and practice of soil science: the soil as a natural resource*. John Wiley & Sons.

Wickham, H. (2016). *ggplot2: Elegant Graphics for Data Analysis*. Springer-Verlag New York.

Wisotzky, F. (2011). Angewandte Grundwasserchemie, Grundwasserbelastung und Aufbereitung: Grundlagen, Anwendungen und Problemlösungen. *Earth sciences. Springer Berlin, Berlin*, 1.

Wu, Q., Zhang, T., and Liu, Y. (2010). Permafrost temperatures and thickness on the Qinghai-Tibet Plateau. *Global and Planetary Change*, 72(1-2):32–38.

Wuana, R. A. and Okieimen, F. E. (2011). Heavy metals in contaminated soils: a review of sources, chemistry, risks and best available strategies for remediation. *Isrn Ecology*, 2011.

Yershov, E. D. (2004). *General geocryology*. Cambridge university press.

Zhang, T., Barry, R., Knowles, K., Heginbottom, J., and Brown, J. (2008). Statistics and characteristics of permafrost and ground-ice distribution in the Northern Hemisphere. *Polar Geography*, 31(1-2):47–68.

Zimov, S. A., Schuur, E. A., and Chapin, F. S. (2006). Permafrost and the global carbon budget. *Science*, 312(5780):1612–1613.

Appendix

Table 5 Summary of pH, electrical conductivity and hydrogen carbonate data.

Sample	pH	EC (µS/cm)	HCO_3^- (mg/L)	Description
B17-MF-01	7.39	1904	1154	Slump
B17-MF-02	7.30	1896	1129	Slump
B17-MF-03	7.31	1651	812	Slump
B17-MF-04	6.82	685	259	Batagaika River
B17-MF-05	6.60	1285	404	Batagaika River
B17-MF-06	6.90	1937	1198	Slump Outflow
B17-MF-07	6.52	42.5	16.2	Batagaika River
B17-MF-08	7.12	1877	1177	Slump
B17-MF-09	6.75	124	34	Yana River
B17-MF-10	6.90	395	228	Batagaika River
B17-MF-11	6.62	120	36.2	Yana River

Table 6 Summary of dissolved organic carbon (DOC), δ^{13}C-DOC, dissolved nitrogen (DN), DOC / DN ratio, dissolved organic nitrogen (DON), ammonia (NH_4), nitrate (NO_3) and nitrite (NO_2).

Sample	DOC (mg/L)	DN (mg/L)	DOC / DN ratio	DON (mg/L)	NH_4 (mg/L)	NO_3 (mg/L)	NO_2 (mg/L)	Description
B17-MF-01	170	13.4	14.8	9.52	3.89	< 0.014	< 0.04	Slump
B17-MF-02	169	12.6	15.6	8.98	3.30	0.38	< 0.04	Slump
B17-MF-03	158	8.97	20.6	8.40	0.03	0.55	< 0.04	Slump
B17-MF-04	65	5.18	12.7	2.79	0.03	2.36	< 0.04	Batagaika River
B17-MF-05	164	11.9	16.1	8.12	3.79	< 0.014	< 0.04	Batagaika River
B17-MF-06	172	13.4	14.9	9.74	3.42	0.25	< 0.04	Slump Outflow
B17-MF-07	4.87	< 0.5	-	< 0.5	0.03	0.05	< 0.04	Batagaika River
B17-MF-08	173	13.8	14.6	10.07	3.72	0.02	< 0.04	Slump
B17-MF-09	4.38	< 0.5	-	< 0.5	< 0.01	0.12	< 0.04	Yana River
B17-MF-10	18.3	2.36	9.09	0.64	0.01	1.71	< 0.04	Batagaika River
B17-MF-11	4.25	< 0.5	-	< 0.5	< 0.01	0.06	< 0.04	Yana River

Table 7 Summary of major anion and cation concentrations Mg^{2+}, Ca^{2+}, Na^{+}, K^{+}, Cl^{-} and SO_4^{2-}.

Sample	Mg^{2+} (mg/L)	Ca^{2+} (mg/L)	Na^{+} (mg/L)	K^{+} (mg/L)	Cl^{-} (mg/L)	SO_4^{2-} (mg/L)	Description
B17-MF-01	165	176	84	5.41	58.4	158	Slump
B17-MF-02	154	176	89.5	5.41	64.6	141	Slump
B17-MF-03	128	140	93.7	4.65	67.3	221	Slump
B17-MF-04	38.6	80.9	26.8	2.73	22.9	105	Batagaika River
B17-MF-05	83.5	110	81.9	6.63	69.4	264	Batagaika River
B17-MF-06	159	178	88.8	5.38	66.8	113	Slump Outflow
B17-MF-07	1.7	4.37	1.63	0.44	1.15	4.62	Batagaika River
B17-MF-08	155	170	86.9	5.04	64.4	128	Slump
B17-MF-09	5.1	15.3	2.65	0.76	1.46	24.5	Yana River
B17-MF-10	18.9	60.9	8.75	1.47	3.21	17.9	Batagaika River
B17-MF-11	4.9	14.8	2.48	0.73	1.42	24.4	Yana River

Table 8 Summary of element concentrations Al, Ba, Fe, Mn, P, Si, Sr, Ni, Cu, Zn.

Sample	Al (µg/L)	Ba (µg/L)	Fe (µg/L)	Mn (µg/L)	P (mg/L)	Si (mg/L)	Sr (µg/L)	Ni (µg/L)	Cu (µg/L)	Zn (µg/L)	Description
B17-MF-01	<20	42	2279	7330	0.16	5.33	1090	32	<20	77	Slump
B17-MF-02	<20	48	1819	6572	<0.1	5.27	1081	24	<20	101	Slump
B17-MF-03	<20	59	1006	4915	<0.1	4.66	903	32	24	79	Slump
B17-MF-04	67	77	159	<20	<0.1	2.39	456	<20	<20	20	Batagaika River
B17-MF-05	54	57	762	2626	0.21	2.57	630	25	<20	31	Batagaika River
B17-MF-06	<20	53	2030	7157	0.10	5.49	1110	25	<20	29	Slump Outflow
B17-MF-07	<20	<20	41	<20	<0.1	1.99	26.5	<20	<20	86	Batagaika River
B17-MF-08	<20	49	2234	6283	0.11	5.27	1070	26	<20	30	Slump
B17-MF-09	<20	<20	44	<20	<0.1	2.34	142	<20	<20	<20	Yana River
B17-MF-10	85	36	196	<20	<0.1	2.44	284	<20	<20	35	Batagaika River
B17-MF-11	<20	<20	25	<20	<0.1	2.41	139	<20	<20	<20	Yana River

Table 9 Summary of δ^{13}C-DOC and δ^{13}C-TOC isotope data in ‰vs. VPDB.

Sample	δ^{13}C-DOC (‰VPDB)	δ^{13}C-TOC (‰VPDB)	Description
B17-MF-01	-26.01	-24.59	Slump
B17-MF-02	-26.10	-24.59	Slump
B17-MF-03	-26.13	-24.17	Slump
B17-MF-04	-26.14	-25.36	Batagaika River
B17-MF-05	-25.91	-25.26	Batagaika River
B17-MF-06	-25.97	-24.36	Slump Outflow
B17-MF-07	-27.37	-	Batagaika River
B17-MF-08	-25.99	-24.27	Slump
B17-MF-09	-27.57	-26.24	Yana River
B17-MF-10	-26.35	-24.82	Batagaika River
B17-MF-11	-27.60	-26.43	Yana River

Table 10 Summary of stable water isotopes (δ^{18}O, δ^{2}H and d excess), minimum, mean, maximum values, standard deviation (sd), slope, intercept and R^2 for the category all samples, Batagaika and Yana River water and slump water. In addition the mean, minimum and maximum values from Vasil'chuk et al. (2017), presenting data from three different ice wedges from the upper Ice complex (Unit III) and data from Opel et al. (2018) from different units as well as rain water and slump surface water.

Group	N	δ^{18}O (‰) min	δ^{18}O (‰) mean	δ^{18}O (‰) max	δ^{18}O (‰) sd	δ^{2}H (‰) min	δ^{2}H (‰) mean	δ^{2}H (‰) max	δ^{2}H (‰) sd	d (‰) min	d (‰) mean	d (‰) max	d (‰) sd	Slope	R^2
All Samples	11	-32.3	-26.7	-19.3	5.58	-243	-202	-146	41.1	5.47	11.5	16.1	3.93	7.4	0.99
Batagaika River	3	-22.6	-21.3	-20.1	1.8	-175	-164	-152	16.3	5.47	6.82	8.17	1.91	8.9	0.99
Yana River	2	-21.3	-21.3	-21.3	0.01	-162	-162	-162	0.07	8.12	8.13	8.14	0.01	10	1.00
Slump	6	-32.3	-31.5	-30.5	0.57	-243	-237	-233	3.60	11.2	14.6	16.1	1.78	5.9	0.86
Ice wedge 1	8	-34.8	-34.4	-32.6	-	-270	-265	-247	-	7.34	10.2	14.2	-	-	-
Ice wedge 2	59	-37.2	-35.6	-34.9	-	-290	-276	-259	-	4.12	9.19	13.4	-	-	-
Ice wedge 3	39	-34.8	-34.6	-33.8	-	-272	-266	-255	-	4.16	8.57	13.6	-	-	-
Upper sand unit B17-IW2 (CW)	4	-33.0	-32.8	-32.4	0.25	-250	-247	-242	3.3	13.7	15.1	16.9	1.5	12.5	0.92
B17-IW3 (CW)	2	-32.1	-31.8	-31.6	0.38	-244	-240	-236	5.5	12.9	14.7	16.4	2.4	14.4	1.00
B17-IW4	6	-30.1	-29.8	-29.4	0.22	-229	-225	-212	5.6	10	13.5	22.3	4.1	22.3	0.79
Intrased. ice	3	-32.6	-30.5	-29.2	1.82	-242	-220	-207	19.3	18.7	24.4	28.2	5.1	10.6	0.99
Upper Ice Complex B17-IW5	12	-36.1	-34.8	-33.5	0.86	-280	-271	-260	6.4	6.8	8.1	10.3	0.9	7.41	0.99
B17-IW6	4	-35.5	-34.5	-33.1	0.92	-274	-262	-246	12	8.5	13.8	19.9	4.8	12.9	0.98
Intrased. ice	2	-27.6	-26.1	-24.75	2.04	-198	-195	-191	5.0	6.5	14.5	22.5	11.3	2.44	1.00
Lower Sand B17-IW1	6	-33.3	-33.1	-32.9	0.13	-258	-256	-254	1.5	6.9	8.2	9.4	0.8	9.94	0.72
Intrased. ice	4	-32.5	-32.3	-32.2	0.14	-247	-244	-241	3.2	12.4	14.7	16.8	2.3	20.0	0.77
Other Outflow water	7	-32.2	-31.7	-31.3	0.34	-244	-238	-235	3.1	14.3	14.2	16.1	0.6	8.8	0.97
Rain water	4	-16.8	-14.3	-10.1	2.92	-131	-112	-79.0	23.1	2.3	2.6	2.9	0.2	7.93	1.00

Table 11 Summary of ^{14}C AMS ages of TOC with σ1 and σ2 calibrated ranges.

Sample	Laboratory Nr.	^{14}C (ka BP)	Calibrated age range σ1 (ka BP)	Mean σ1 (ka BP)	Calibrated age range σ2 (ka BP)	Mean σ2 (ka BP)	Description
B17-MF-01	1865.1.1	35.485 ± 0.209	39.804 - 40.341	40.073	39.532 - 40.644	40.088	Slump
B17-MF-02	1866.1.1	29.171 ± 0.118	33.265 - 33.611	33.438	33.034 - 33.727	33.381	Slump
B17-MF-03	1867.1.1	31.051 ± 0.137	34.761 - 35.075	34.918	34.622 - 35.266	34.944	Slump
B17-MF-04	1868.1.1	20.122 ± 0.070	24.073 - 24.302	24.188	23.959 - 24.411	24.185	Batagaika River
B17-MF-05	1869.1.1	26.973 ± 0.101	30.952 - 31.135	31.017	30.851 - 31.217	31.034	Batagaika River
B17-MF-06	1870.1.1	36.231 ± 0.222	40.616 - 41.178	40.897	40.326 - 41.396	40.861	Slump Outflow
B17-MF-08	1871.1.1	32.721 ± 0.157	36.368 - 36.827	36.598	36.210 - 37.278	36.729	Slump
B17-MF-09	1872.1.1	15.404 ± 0.059	18.609 - 18.746	18.678	18.539 - 18.805	18.672	Yana River
B17-MF-10	1873.1.1	23.238 ± 0.080	27.412 - 27.591	27.502	27.323 - 27.682	27.503	Batagaika River
B17-MF-11	1874.1.1	14.011 ± 0.057	16.907 - 17.139	17.023	16.733 - 17.254	16.994	Yana River

Table 12 Summary of ^{14}C-DOC AMS ages with σ1 and σ2 calibrated ranges. Subdivided by sample location slump, Batagaika and Yana River.

Sample	Laboratory Nr.	^{14}C-DOC (ka BP)	Calibrated age range σ1 (ka BP)	Mean σ1 (ka BP)	Calibrated age range σ2 (ka BP)	Mean σ2 (ka BP)	Description
B17-MF-01	COL5326.0.1	30.747 ± 0.226	34.458 - 34.897	34.678	34.198 - 35.104	34.651	Slump
B17-MF-05	COL5327.0.1	30.488 ± 0.233	34.229 - 34.671	34.485	34.019 - 34.868	34.444	Batagaika River
B17-MF-06	COL5328.0.1	29.239 ± 0.221	33.222 - 33.719	33.471	32.901 - 33.875	33.388	Slump Outflow
B17-MF-07	COL5329.0.1	1.831 ± 0.047	1.710 - 1.822	1.766	1.624 - 1.875	1.749	Batagaika River
B17-MF-08	COL5330.0.1	23.958 ± 0.134	27.822 - 28.135	27.979	27.723 - 28.349	28.036	Slump
B17-MF-09	COL5331.0.1	0.936 ± 0.057	0.796 - 0.916	0.856	0.732 - 0.952	0.842	Yana River
B17-MF-11	COL5332.0.1	0.890 ± 0.053	0.737 - 0.904	0.821	0.705 - 0.922	0.814	Yana River

Table 13 Summary of the samples wet and dry weight, volumes, dry bulk density and sediment content. Subdivided by sample location Slump, Batagaika and Yana River.

Sample	Wet Weight (g)	Dry Weight (g)	Volume (ml)	Volume of suspended matter (ml)	Dry Bulk Density (g/cm^3)	Sediment contet (%)	Description
B17-MF-01	1641	987	1035	700	1.41	60.1	Slump
B17-MF-02	1571	892	1030	700	1.28	56.8	Slump
B17-MF-03	1623	1028	1000	700	1.47	63.4	Slump
B17-MF-04	981	2.55	1020	-	-	0.26	Batagaika River
B17-MF-05	1008	4.35	1030	-	-	0.43	Batagaika River
B17-MF-06	1448	770	990	500	1.54	53.2	Slump Outflow
B17-MF-07	1031	1.55	1060	-	-	0.15	Batagaika River
B17-MF-08	1552	868	1030	700	1.24	55.9	Slump
B17-MF-09	1020	1.55	1040	-	-	0.15	Yana River
B17-MF-10	1009	12.7	1030	10	1.28	1.26	Batagaika River
B17-MF-11	1030	1.75	1050	-	-	0.17	Yana River